ELSEVIER

Marine Geology 230 (2006) 275–303

MARINE GEOLOGY
INTERNATIONAL JOURNAL OF MARINE GEOLOGY, GEOCHEMISTRY AND GEOPHYSICS

www.elsevier.com/locate/margeo

Facies system of the Eastern Barents Sea since the last glaciation to present

Ivar Murdmaa [a,*], Elena Ivanova [a], Jean-Claude Duplessy [b], Michael Levitan [c], Tatyana Khusid [a], Maria Bourtman [a], Galina Alekhina [a], Tatyana Alekseeva [a], Michael Belousov [a], Valentina Serova [a]

[a] *P.P. Shirshov Institute of Oceanology, Russian Academy of Sciences, 36 Nakhimovskii prosp., Moscow 117997, Russia*
[b] *Laboratoire des Sciences du Climat et de l'Environnement, Laboratoire mixte CNRS-CEA, Parc du CNRS, 91198 Gif sur Yvette Cedex, France*
[c] *Vernadsky Institute of Geochemistry and Analytical Chemistry, Russian Academy of Sciences, Kosygina ul. 1, 119991 Moscow, Russia*

Received 7 July 2005; received in revised form 31 May 2006; accepted 2 June 2006

Abstract

Twenty-two sediment cores raised from the central and eastern parts of the Barents Sea have been studied to reconstruct the evolution of the facies system since the Late Weichselian glaciation. Multiproxy records reveal four lithostratigraphic units, which reflect major development stages of paleoenvironments. Age control is provided by 23 AMS ^{14}C dates for Holocene sections of four cores. Continental moraine deposits of the last glaciation are overlain by proximal glaciomarine facies of the initial deglaciation phase. During this phase, the Barents Sea ice sheet detached from the ground resulting in seawater penetration into troughs, iceberg calving, deposition of IRD and fine-grained glacier meltwater load in newly formed marine basins. The main deglaciation phase is characterized by pulsed sedimentation from various gravity flows resulting in accumulation of distal glaciomarine facies comprising laminated clay and sand sequences with minor IRD. Redistribution of fine-grained suspended matter by bottom currents and brine-induced nepheloid flows combined with biogenic processes and minor ice rafting caused facies diversity of the Holocene marine sediments. The Holocene facies of shelf depressions reflect rather high, but variable productivity responding to climate changes and variations of Atlantic water inflow into the Barents Sea.

Keywords: Barents Sea; facies; sedimentary record; Late Weichselian; deglaciation; Holocene

1. Introduction

The Barents Sea (BS) history since the Last Glacial Maximum comprises dramatic paleoenvironmental changes: destruction of the BS ice sheet, varying penetration of Atlantic water, variations in terrigenous material supply, biological productivity, and bottom current activity. Late Quaternary sedimentary records have been discussed in terms of paleoceanography (e.g. Polyak and Solheim, 1994; Polyak and Mikhailov, 1996; Lubinski et al., 1996, 2001; Duplessy et al., 2001, 2005; Ivanova et al., 2002). However, less attention was paid to lithological aspects (e.g. Elverhoi and Solheim, 1983; Elverhoi et al., 1989, 1993; Vorren et al., 1989; Gataullin et al., 1993, 2001; Gurevich, 1995; Polyak et al., 1995; Murdmaa and Ivanova, 1999; Bogdanov et al., 2001; Pavlidis et al., 2001, 2005). Such problems of terrigenous sedimentation, as material sources, transport mechanisms, and deposition modes at different development

* Corresponding author.
E-mail address: murdmaa@mail.ru (I. Murdmaa).

0025-3227/$ - see front matter © 2006 Elsevier B.V. All rights reserved.
doi:10.1016/j.margeo.2006.06.001

stages of the post-glacial BS are still insufficiently studied. The facies diversity of the Late Weichselian to recent sedimentary cover on the BS shelf described by many authors needs more comprehensive explanation in terms of paleoenvironments.

In this paper, we used 22 cores raised from shelf depressions during cruises of the R.V. "Akademik Sergei Vavilov" (1997–1998) to reconstruct the sedimentary history of the central and eastern BS since the initial destruction of the grounded ice sheet, which covered it during the last glaciation (e.g. Thiede and Mangerud, 1999; Svendsen et al., 2004a,b). We focused our research on relatively complete sedimentary records recovered from the BS shelf depressions, whereas only a brief overview of sedimentary environments on submarine rises is given to understand the facies system as a whole.

2. Physiographic and oceanographic setting

The BS is a typical glacier-affected epicontinental shelf with a rough topography (Fig. 1). It is surrounded by Spitsbergen and Franz Josef Land archipelagoes in the north, by the Novaya Zemlya archipelago in the east, and by the northern Europe in the south. The Franz Victoria Trough separates Spitsbergen from Franz Josef Land. A wide passage exists between the Franz Josef Land and Novaya Zemlya, with the Sedov trough opening into the St. Anna Trough (Kara Sea) in its central part. The shallow Karskie Vorota Strait connects the Barents and Kara seas in the south–east (Fig. 1).

Wide offshore shoals of Pechora Sea, Kanin and Murmansk banks separate the eastern BS basin from the continent in the south, while only very narrow offshore shoals exist around the archipelagoes. The bottom

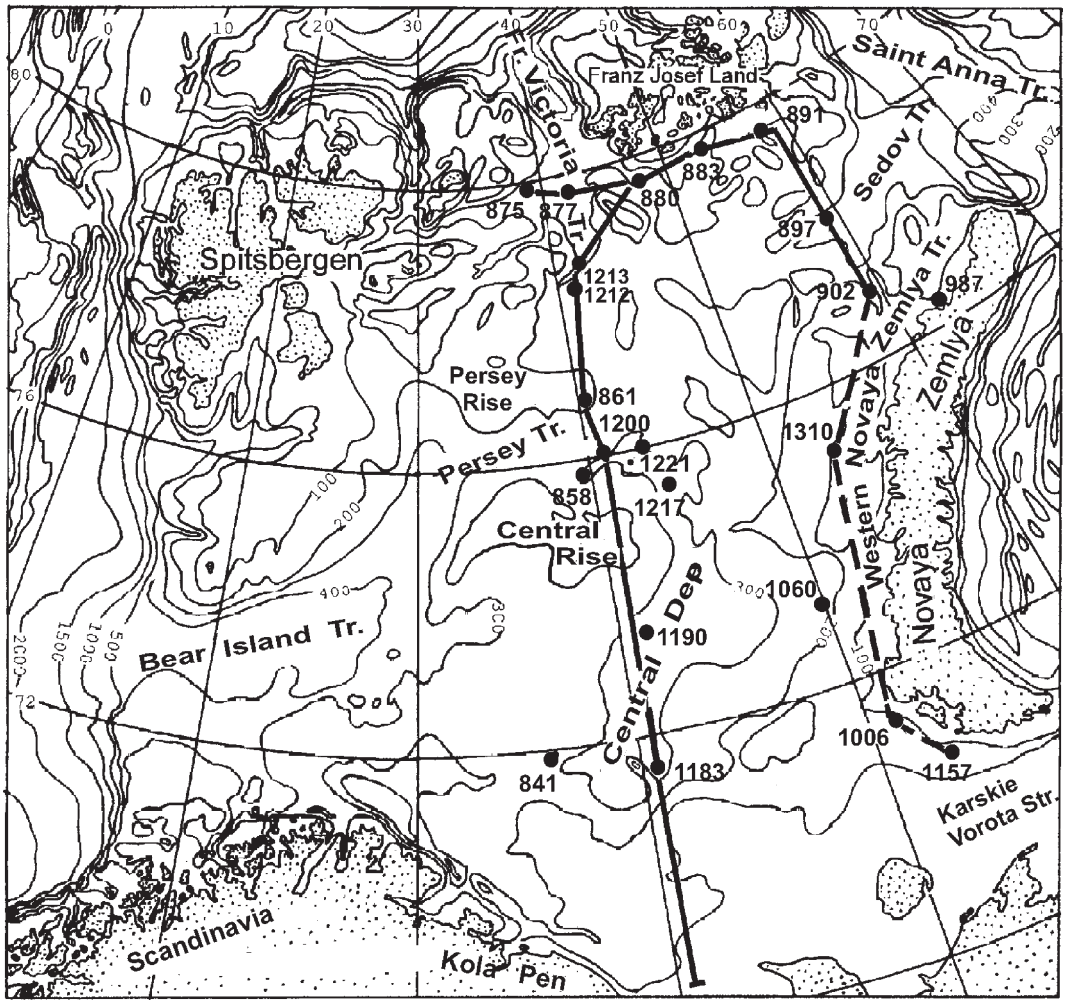

Fig. 1. Bathymetric map of the Barents Sea with location of *R/V Akademic Sergei Vavilov* cores considered in this paper, and with three transects shown in Figs. 2–4.

topography of the eastern BS includes several shallow submarine rises, with water depth <200 m over their summits: Central, Persey, Albanov, Gusinaya (Geese), Admiralty banks and some other. The Central Deep, with depth up to 350 m extends from 71°N to 78°N in the east. Persey Trough separates Central and Persey banks (Figs. 1 and 2). The discontinuous Western Novaya Zemlya Trench extends along the western coast of the archipelago. Several local troughs with maximum depth of almost 500 m are crossed by our core transects (Figs. 2–4).

The modern hydrology of the BS is controlled by the interaction between cold low-salinity Arctic water and warmer high-salinity Atlantic water. Arctic water enters the BS through passages between the archipelagoes in the north. It carries pack ice from the Transpolar Drift during winter. Atlantic water penetrates the BS as the North Cape surface current in the south and as intermediate water flows in the north, through the Franz Victoria, St. Anna and Sedov troughs. The boundary between transformed Atlantic water and Arctic water represents the Polar front. It migrates between 74° and 76°N and constitutes a major sinking and mixing area (Djenynk, 1990; Byshev et al., 2001).

Sea-ice conditions are characterized by strong seasonal and multiannual variability in position of the ice margin (Zubakin, 1990). During the coldest years, the area east of 40°E is ice-covered up to north-eastern Kola Peninsula coast in winter, whereas the winter ice margin occurs at about 76°N during the warmest years. The July to October ice margin is commonly found north of 80°N. However, the summer ice limit may reach 76°N during years of extensive ice cover (e.g. Vinje, 1985). Therefore, almost the entire eastern BS represents a seasonal sea-ice zone without any stable marginal ice zones (MIZ). Permanent annual ice-free zone related to the warm North Cape current extends westward of about 40°E between the Scandinavian coast and the Polar front.

3. Geological setting

The Upper Quaternary sediment cover of the eastern and central BS considered here unconformably overlies the gently dipping and faulted Upper Paleozoic–Mesozoic sedimentary sequence (up to 12–15 km thick) that infills the East Barents Sea rift beneath the Central Deep, and makes up surrounding rises

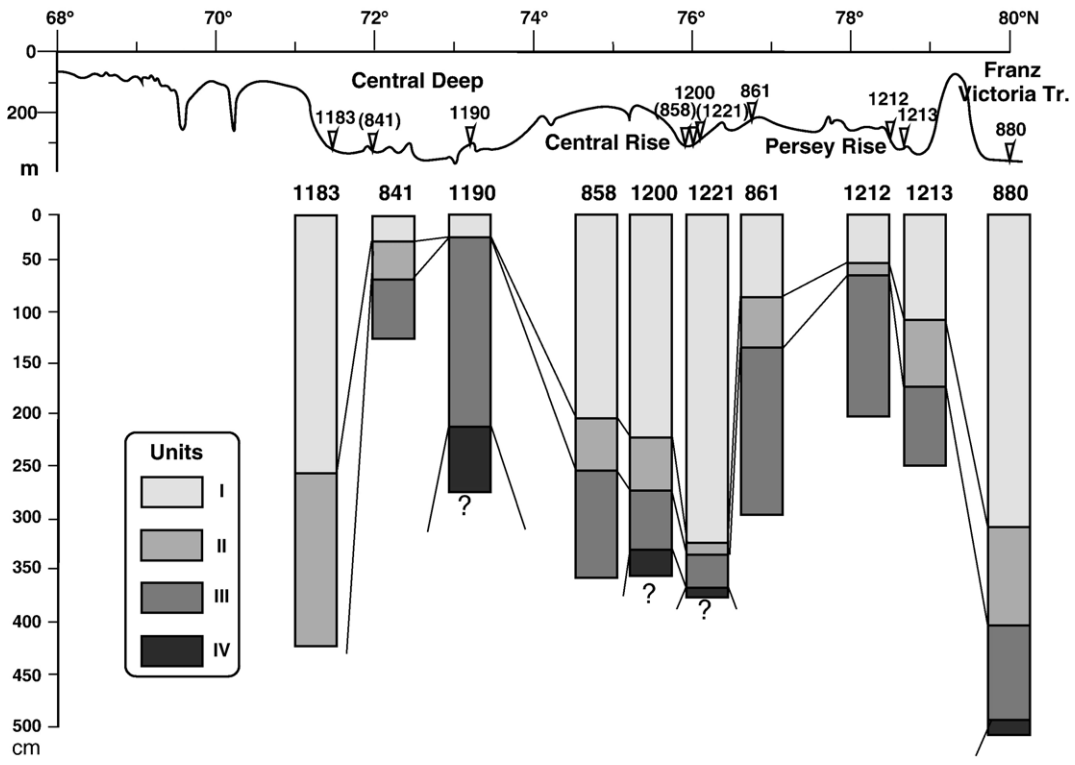

Fig. 2. Western S–N transect along about 40–41°E. Location of cores is shown in the generalized bathymetric profile above (numbers in parentheses indicate cores aside from the profile); cores with correlation of four lithostratigraphic units are placed below.

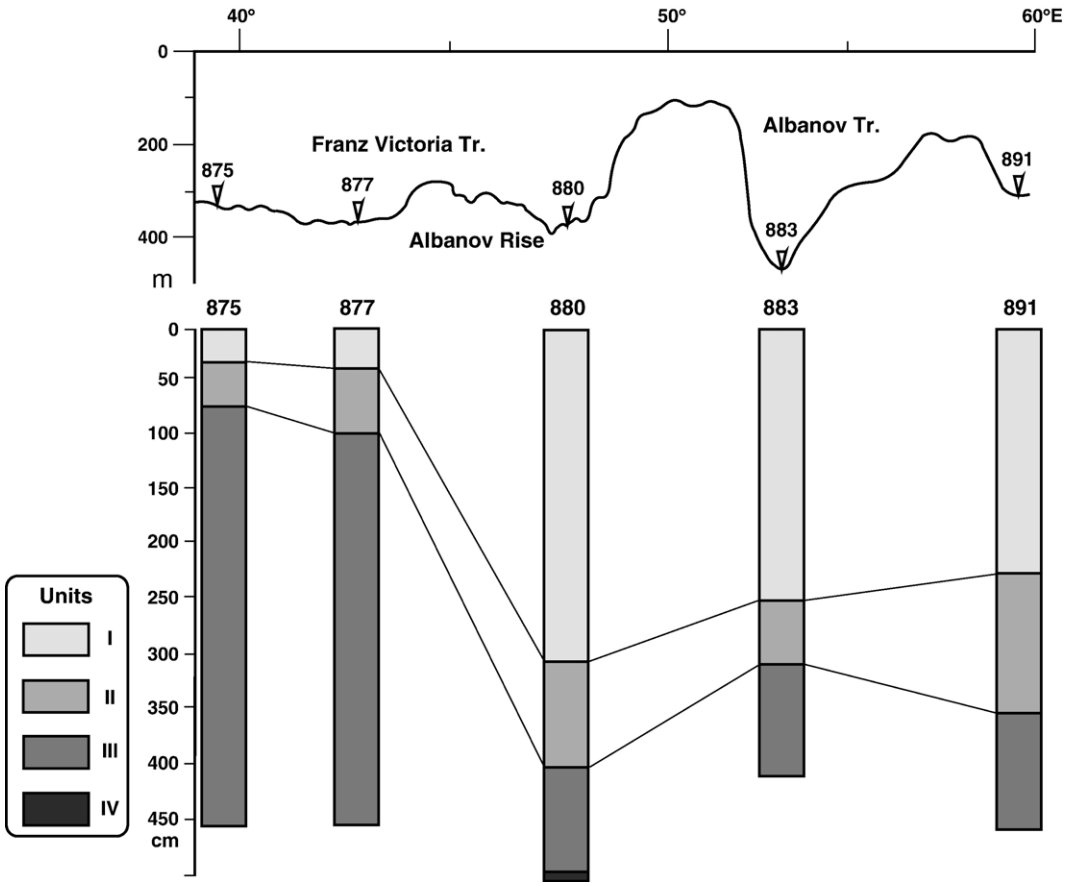

Fig. 3. Northern W–E transect along 79°45′–79°57′N. Location of cores is shown in the generalized bathymetric profile above; cores with correlation of four lithostratigraphic units are placed below.

(Sigmond, 1992; Alekhin, 1993; Ignatenko and Cheredeev, 1993; Elverhoi et al., 1995). Mesozoic sedimentary rocks and Cretaceous plateau basalts form the acoustic basement of the northeastern BS around the Franz Josef Land (Solheim et al., 1998).

Extensive investigations during last decades, including seismic profiling, sediment coring and drilling, resulted in a common agreement that a major grounded Late Weichselian ice sheet covered the Barents Sea shelf and surrounding archipelagoes (e.g. Vorren, 1992; Sættem et al., 1992; Lambeck, 1995; Vorren and Laberg, 1996; Thiede and Mangerud, 1999; Polyak et al., 2000; Gataullin et al., 2001; Svendsen et al., 1999, 2004a,b). Moraine deposits (glacial till) of the Last Glacial Maximum (LGM) directly overly the Upper Regional Unconformity (URU) at the top of Mesozoic bedrocks, as it is demonstrated by seismic records and by drill holes (e.g. Gataullin et al., 1993, 2001; Polyak and Mikhailov, 1996; Polyak et al., 1997; Murdmaa and Ivanova, 1999). This indicates a removal of older soft sediments by glacial erosion during LGM. However, some relics of marine sediments deposited prior to the last glaciation possibly escaped the glacier erosion (Pavlidis and Polyakova, 1997). Middle Weichselian marine sediments and underlying glacial till are recovered in the southern Pechora Sea aside of the Late Weichselian ice sheet limits (Polyak et al., 2000; Gataullin et al., 2001).

According to seismic reflection, coring, and drilling data, the post-glacial (last deglaciation and Holocene) sediments described in this paper cover the moraine relief as a discontinuous blanket interrupted on the submarine rises and thickening in local depressions (e.g. Gataullin et al., 1993; Polyak and Mikhailov, 1996; Murdmaa and Ivanova, 1999).

4. Materials and methods

This study is based on 22 gravity cores collected from shelf depressions of the central and eastern BS during *R/V Akademik Sergei Vavilov* (ASV) cruises 11, 13, and 14 in 1997–1998 (Table 1, Fig. 1). The set of 19

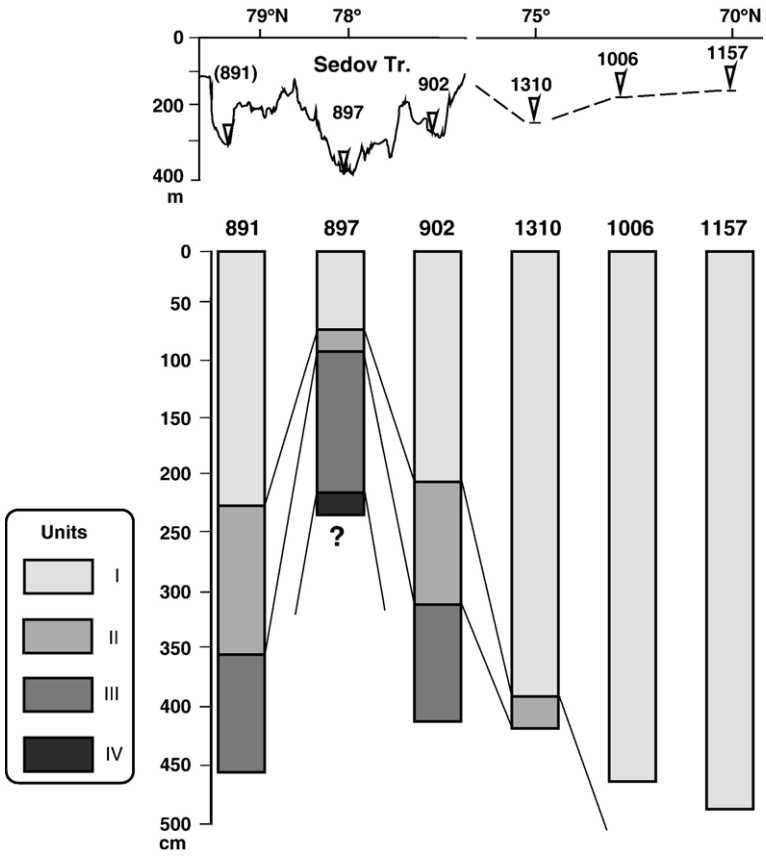

Fig. 4. Eastern N–S transect along about 60°E, with location of cores in the bathymetric profile above, continued from Core ASV 902 to the south with cores ASV 1310, ASV 1006, and ASV 1157 from the Western Novaya Zemlya Trench. Water depths at these coring stations are united by dashed line above. Correlation of lithostratigraphic units recovered in the cores is placed below.

gravity cores constitutes three transects (Fig. 1). A *western* N–S transect (Fig. 2) proceeds from the eastern branch of the Franz Victoria Trough to the southern edge of the Central Deep. A *northern* W–E transect at about 80°N latitude (Fig. 3) follows eastward from the central and eastern branches of the Franz Victoria Trough to a trough south of eastern Franz Josef Land. An *eastern* transect (Fig. 4) crosses at 60°E the passage between Franz Josef Land and Novaya Zemlya and continues to the south along the Western Novaya Zemlya Trough.

We also consider a visual description of about 20 grab samples, along with numerous publications on surface sediments of the BS (e.g. Gurevich, 1995), to characterize briefly the facies of submarine rise summits.

The cores were described and sampled aboard the ship. The thickness of each sample was 1–2 cm. The sampling interval varies between 5 and 20 cm. The grain-size distribution was measured in six selected cores following the combined sieving (>0.05 mm fractions), decantation (0.05–0.01 mm fraction), and pipette (0.01–0.005 mm, 0.005–0.001 mm, and <0.001 mm fractions) method developed by Petelin (1967). Besides, the coarse fractions (>1 mm, 1–0.1 mm, and 0.1–0.05 mm) were determined at 5-cm intervals. In order to adapt the decimal scale of size fractions used in Russia to the western classification based on a logarithmical scale, we called clay the fraction <0.005 mm, silt the fraction between 0.05 and 0.005 mm, sand the fraction between 1 and 0.05 mm, and gravel the fraction between 10 and 1 mm. We also use the term ‘pelite’ for the sum of fractions <0.01 mm.

The 0.1–0.05 mm size fraction was subdivided into heavy and light components in bromoform (density 2.9 g/cm^3), and the heavy grains were analysed by routine immersion method. Not less than 300 mineral grains were counted in each specimen. Seven most widespread transparent terrigenous minerals were used to characterize variations of heavy mineral assemblages: hornblende, clinopyroxene, epidote, garnet, zircon,

apatite, and titanium minerals (sphene, rutile, anatase, and some other). The sum of these 7 minerals and 'other' more rare transparent ones was equalized to 100%, and proportion of each was calculated.

We determined clay minerals using a DRON-2 X-ray diffractometer and evaluated their relative content according to Biscaye (1965) . The total organic carbon (TOC) was measured using carbon analyzer AN-7529.

Two-centimeter samples were taken every 5 cm in selected cores for foraminiferal analysis. When available, 200–300 tests of benthic foraminifera were identified in a split aliquot of the sediment fraction >100 μm. All planktic foraminifers were identified and counted.

Oxygen and carbon isotopes were measured on the planktic and benthic foraminiferal tests using a Finnigan MAT 251 mass spectrometer; NBS 19 and NBS 18 were used as reference standards to ensure a proper calibration on a large range of delta ^{18}O values. 23 AMS dates were obtained in 4 cores by the Tandetron of Gif sur Yvette (Table 2). ^{14}C ages were converted into calendar ages using the calibration of Stuiver and Reimer (1993).

Fragments of seismic reflection records at coring stations demonstrated in this paper were obtained by geophysical teams of the *R/V Akademik Sergei Vavilov*

Table 1
Characteristics of sediment cores from the eastern Barents Sea

Station, ASV no.	Coordinates		Water depth, (m)	Core length, (m)	Thickness of units, (m)		
	N	E			I	II	III
841	71°56.6′	37°03.6′	290	1.26	0.30	0.40	0.56
858	75°50.6′	39°54.8′	312	3.56	2.07	0.49	1.00
861	76°43.0′	40°05.2′	196	2.94	0.86	0.44	1.64
875	79°56.6′	39°48.4′	315	4.56	0.35	0.41	3.80
877	79°55.0′	42°29.7′	358	4.20	0.10	0.30	3.80
880	79°55.5′	47°08.2′	388	5.08	3.10	0.94	0.90*
883	79°49.9′	53°01.4′	457	4.17	2.55	0.60	1.02
891	79°29.3′	59°06.3′	315	4.63	2.28	1.30	1.05
897	78°06.0′	59°56.2′	365	2.31	0.72	0.14	1.45
902	76°51.0′	59°58.6′	268	3.85	2.90	0.24	0.71
1006	71°07.4′	52°00.9′	182	4.45	4.45	–	–
1060	78°21.9′	49°50.4′	252	2.95	1.50	0.34	1.11
1157	70°35′	52°48′	169	4.86	4.86	–	–
11832	71°28.3′	40°48.3′	330	4.17	2.63	1.54	–
1190	73°12.4′	40°56.4′	316	2.76	0.23	=	2.53*
1200	75°54.4′	41°00.5′	308	3.60	2.25	0.47	1.88*
1212	78°30.6′	40°57.1′	289	2.04	0.12	0.48	1.44
1213	78°39.1′	4I°04.0′	326	2.50	1.12	0.59	0.79
1217	75°37.6′	45°42.6′	313	2.12	1.03	0.27	1.09
1221	75°59.8′	42°47.9′	357	3.75	3.26	0.03	0.49*
1302	75°39.5′	46°09.7′	306	2.70	0.78	0.39	1.53
1310	75°06.1′	53°21.7′	228	4.20	3.89	0.31	–

*Total thickness of Unit III, as Unit IV is recovered below: (–) unit is not recovered; (=) unit is missing (hiatus).

Table 2
AMS rediocarbon datings (yr)

Lab Code Gif	Depth in core (cm)	^{14}C age (yr BP)	Error 1 sigma (yr)	Cal. age (yr BP)	Species
ASV 880					
99457	25	1550	60	1104	*Yoldiella lucida*
99385	46	2440	60	2082	*Yoldiella lenticula*
99386	166	6560	80	7081	*Yoldiella fraterna*
99458	216	7420	80	7866	*Yoldiella* spp.
99387	266	8830	90	9282	*Yoldiella fraterna*
99388	305	9150	90	9814	*Yoldiella fraterna*
ASV 1200					
99802	110	5810	70	6225	*Yoldiella* sp.
99803	120	6180	60	6607	*mixed benthic forams*
99804	165	6770	70	7300	*Yoldiella fraterna*
99805	195	9220	80	9981	*Yoldiella lucida*
99806	205	9450	80	10082	*Yoldiella* sp.
99807	210	9550	80	10331	*Yoldiella intermedia*
ASV 1183					
100083	218	9820	100	10707	*Yoldia* sp.
ASV 1157					
99 635	13	840	60	507	*Macoma calcarea*
99 636	50	1900	60	1367	*Tridonta borealis*
99 637	165	3 910	70	3773	*Macoma calcarea*
99 638	338	6 890	90	7423	*Leda* sp.
99 639	355	7 290	90	7683	*Macoma calcarea*
99 640	378	7 600	80	7991	*Macoma calcarea*
99 641	393	8 130	90	8498	*Macoma calcarea*
99 642	398	8 160	90	8529	*Macoma calcarea*
99 643	423	8 570	100	9079	*Pontlandia artica*
99 644	440	8 970	90	9535	*Macoma calcarea*

cruises using the high-frequency Atlas Electronic Parasound seismic profiler (L. Merklin, O. Levchenko, and A. Byakov, unpublished data).

5. Results

5.1. Lithostratigraphy and facies of shelf depression sediments

Seismic profiles and coring data show that more or less continuous Late Weichselian to Holocene sedimentary records can only be recovered from BS shelf depressions, whereas the post-glacial sediment cover practically wedges out on submarine rises (e.g. Gataullin et al., 1993; Gurevich, 1995; Polyak and Mikhailov, 1996; Murdmaa and Ivanova, 1999; Pavlidis et al., 2001).

Four lithostratigraphic units can be recognized in the Upper Quaternary sediment sequences recovered from the shelf depressions (Figs. 2–4).

5.1.1. Unit IV: glacial diamicton (Late Weichselian Glaciation)

Unit IV is represented by the short (14 cm) core catcher sample of core ASV 880 from the south-eastern branch of the Franz Victoria Trough (Figs. 5 and 6). It consists of dark gray very stiff diamicton, a disordered non-stratified mixture of all size fractions from large pebbles to finest clay. Abundant angular or subangular rock fragments with a seldom orientation, up to 12 cm in size, consist of organic-rich black shale similar to that of Triassic age on nearby islands (Solheim et al., 1998). Extremely low water content (18%) and low-salinity pore water (13‰, Murdmaa et al., 1998; Bogdanov et al., 2001) confirm that this basal layer is a continental glacial till (Figs. 7–9).

A similar stiff coarse-grained diamicton probably representing Unit IV is also recovered at the bottom of cores ASV 1200 and ASV 1221 from the Persey Trough, ASV 1190 from the Central Deep (Fig. 2), and ASV 897 from the Sedov Trough (Fig. 4).

5.1.2. Unit III: proximal glaciomarine facies (initial deglaciation phase)

Unit III is an interval of gray to dark gray sandy silty clay with gravel and scattered pebbles that differs from the underlying till by a finer grain size (higher clay and lower coarse fraction content), rare occurrences of benthic and planktic foraminifers, and pore water salinity close to that of seawater (28–30‰). Although massive non-stratified sedimentary structures prevail, we observed indistinct stratification resulting from the presence of layers enriched in gravel- and pebble-size rock fragments or stiff clay clasts.

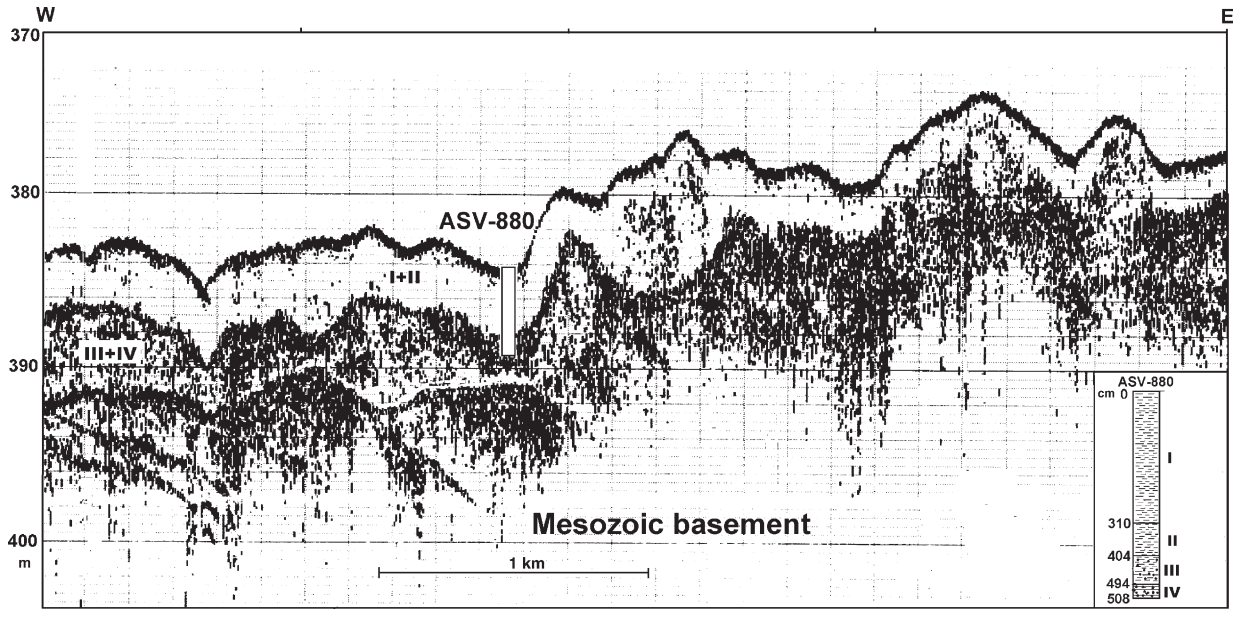

Fig. 5. *Parasound* seismic profile across the ASV 880 site (Franz Victoria Trough, for location see Figs. 1–3) showing the upper acoustically transparent unit corresponding to lithostratigraphic units I+II underlain by the incoherently reflective (chaotic) sequence of Units III+IV, which unconformably overly Mesozoic sedimentary rocks of the acoustic basement. Modified from (Pavlidis et al., 2005). Note, core ASV 880 penetrated the transparent seismic units I+II, and recovered the uppermost part of opaque units III+IV with chaotic reflections.

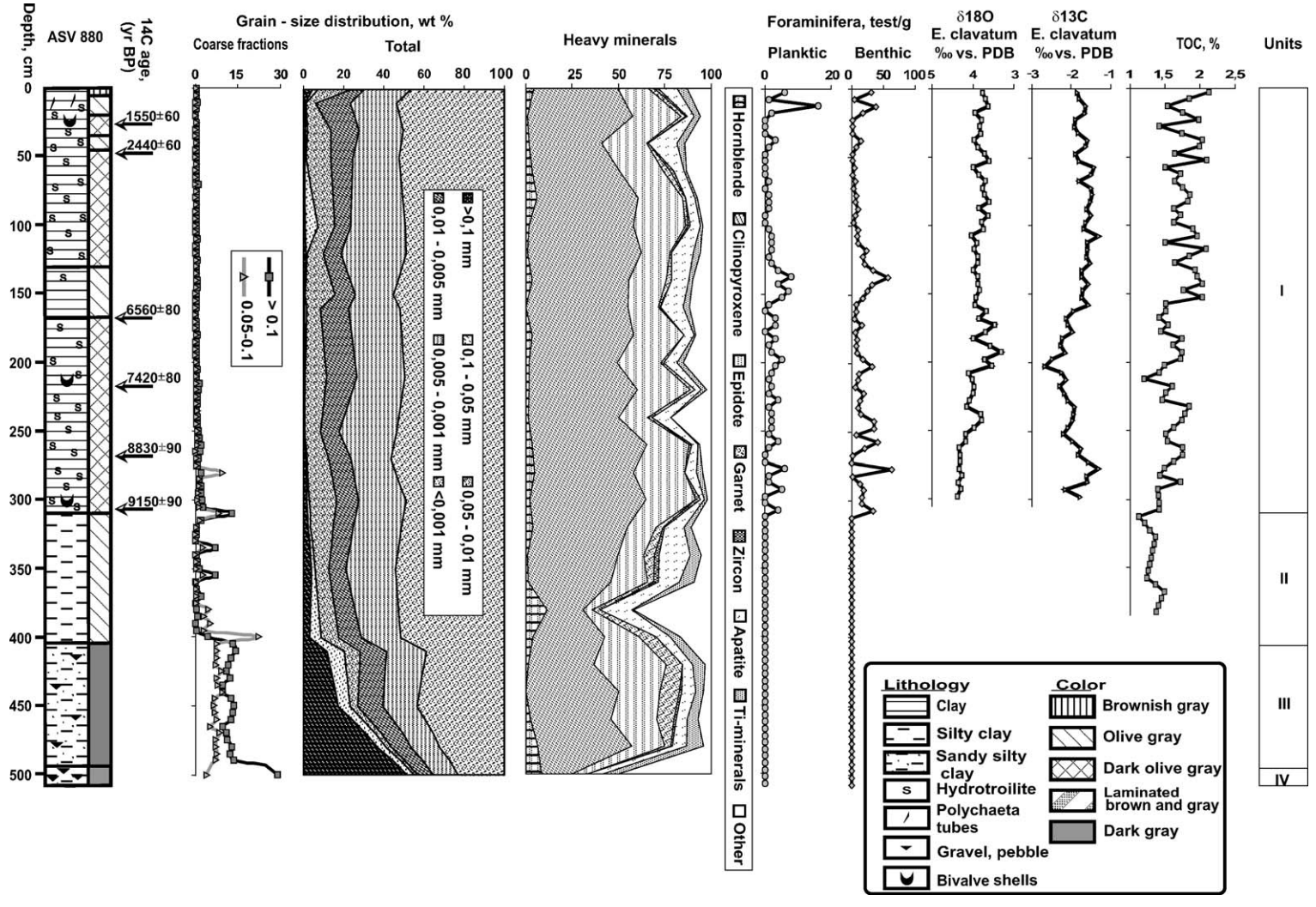

Fig. 6. Core ASV 880 from the Franz Victoria Trough (for location see Figs. 1 and 2) showing lithology of sediments, ^{14}C dates, distribution patterns of coarse fractions, total grain size, heavy minerals, planktic and benthic foraminiferal number, stable isotopes, and TOC.

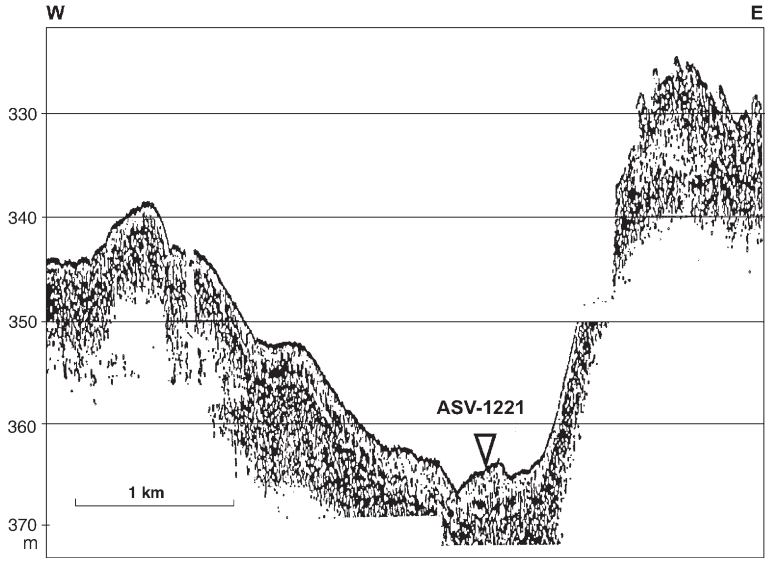

Fig. 7. *Parasound* seismic profile across a valley in the Persey Trough at site of Core ASV 1221 (for location see Figs. 1 and 2). The upper transparent layer corresponds to lithostratigraphic Unit I, and the underlying incoherently reflective layer with chaotic reflections is interpreted as Units IV+III. Unit II is reduced to a ferruginous hardground at the hiatus surface. Note, thickness of the Unit I increases from local rises (moraine mounds) towards the axial valley, where ASV 1221 was raised.

The thickness of Unit III varies from about 0.9 m to more than 3.8 m in the studied cores (Table 1, Figs. 2–4).

As shown in the seismic record across the ASV 880 site (Fig. 5), the incoherently reflective seismostratigraphic unit corresponding to lithostratigraphic units III and IV directly overlies the Mesozoic acoustic basement.

5.1.3. Unit II: distal glaciomarine facies (main deglaciation phase)

Unit II is expressed in seismic records by two major seismic facies, both interpreted by coring data. One is a thick (up to 100 m), acoustically stratified gently undulating sequence widespread in the southern part of the study area (e.g. Gataullin et al., 1993, 2001). It is illustrated by seismic records at sites ASV 1183 (Fig. 10), ASV 1310 (Fig. 12), and ASV 1157 (Fig. 14), where the stratified sequence is 5–20 m thick.

Core ASV 1183 penetrated the upper semi-transparent part of Unit II (Fig. 10). The sediment is an extremely fine-grained homogeneous dusky brown clay that contains up to 92% of clay fraction (Fig. 11). In the seismic profile, a strong reflector lies just below the bottom of Core ASV 1183. It separates the clay layer from the strongly stratified opaque seismic unit, which is possibly a sequence of alternating sand and mud interbeds. The seismic profile (Fig. 10) exhibits meter-scale undulation of the stratified sequence. The undulation corresponds to the surface topography of underlying Units IV+III, demonstrating draped or on-lapping geometry of the Unit II strata.

Similar seismic patterns are recorded below the Western Novaya Zemlya Trough, at site ASV 1310 (Fig. 13). This core recovered below the Holocene layer a sequence of alternating coarse sand and laminated sandy mud beds (Fig. 14) that corresponds to the top of the stratified seismostratigraphic unit, and is attributed to Unit II. Sediment colors vary from gray and light gray to brown and dark brown. A stiff rusty brown ferruginous hardground occurs at the top of a sandy silty mud bed indicating a hiatus surface.

In Franz Victoria, Persey, Albanov, and Sedov troughs, the cores recover a thin (less than 1 m) Unit II (Figs. 2–4). It corresponds to the seismic facies indistinguishable from the upper acoustically transparent Holocene seismic unit (Figs. 5 and 7). In some cores (e.g. ASV 1221), Unit II is reduced to a ferruginous hardground at the eroded top of Unit III, and it wedges out on local moraine mounds (e.g. core ASV 1190; Figs. 2 and 9). Two different facies are commonly found. One occurs in the Persey Trough (cores ASV 858 and ASV 1200); it consists of thinly laminated brown and gray silty clay. Another facies is composed of gray or yellowish gray silty clay with indistinct sandy laminae or lenses. It was recovered in the Franz Victoria Trough (cores ASV 875, ASV 877, ASV 880), the Albanov Trough (core ASV 883), a trough southward of the

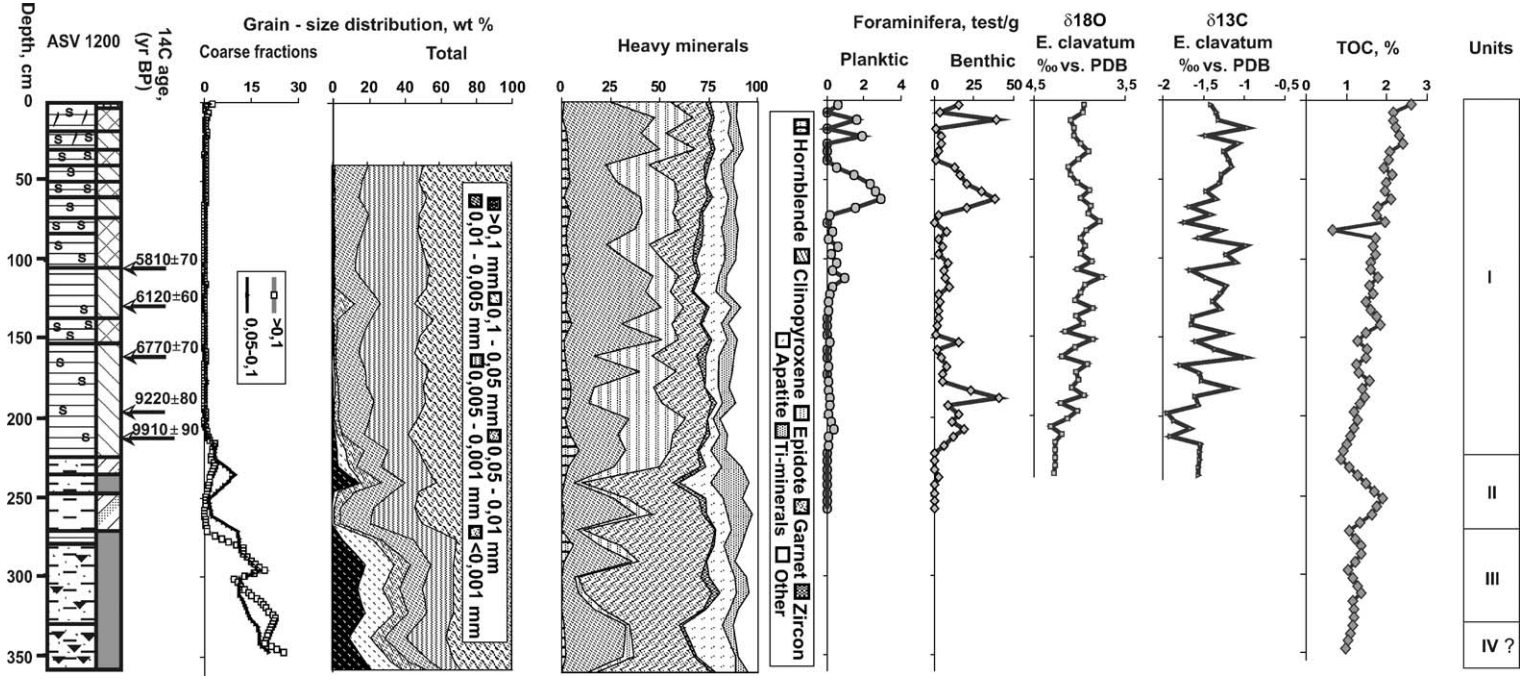

Fig. 8. Core ASV 1200 from the Persey Trough (for location see Figs. 1 and 2) showing lithology of sediments, ^{14}C dates, distribution patterns of coarse fractions, total grain size, heavy minerals, planktic and benthic foraminiferal number, stable isotopes, and TOC. For lithological symbols see Fig. 6.

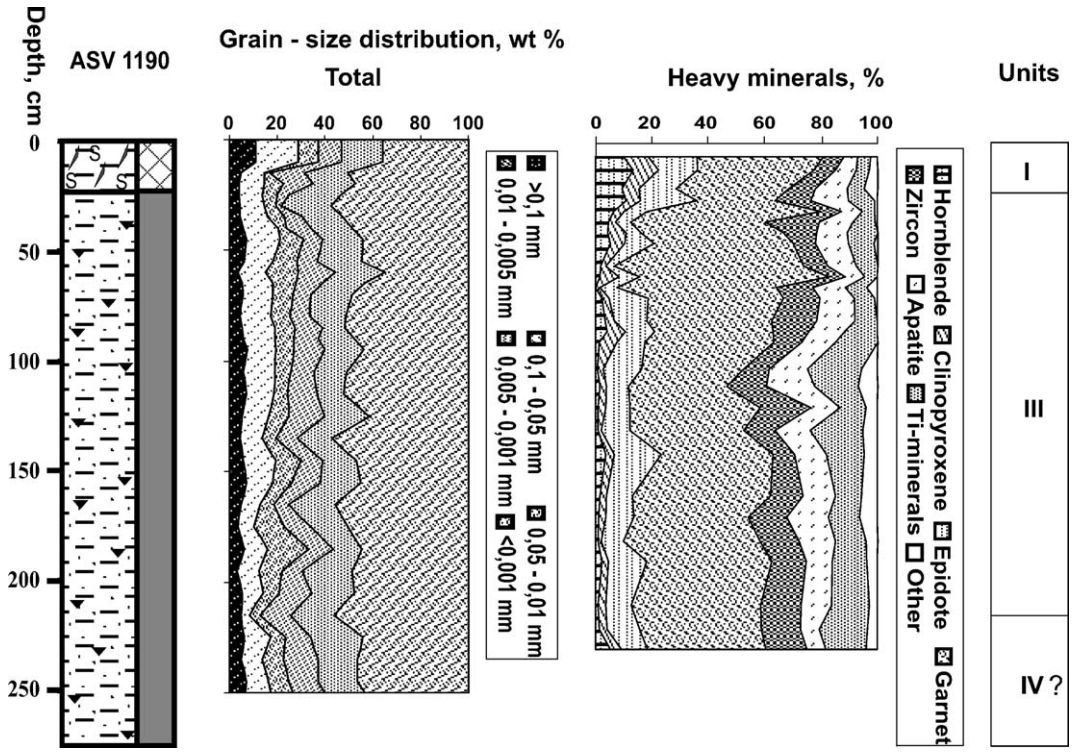

Fig. 9. Core ASV 1190 from the south-western margin of the Central Deep (for location see Figs. 1 and 2) showing lithology of sediments, grain-size and heavy minerals distribution. Note, only a thin (23 cm) Unit I layer directly overlies the relatively fine-grained Unit III, whereas Unit II is likely absent. For lithological symbols, see Fig. 6.

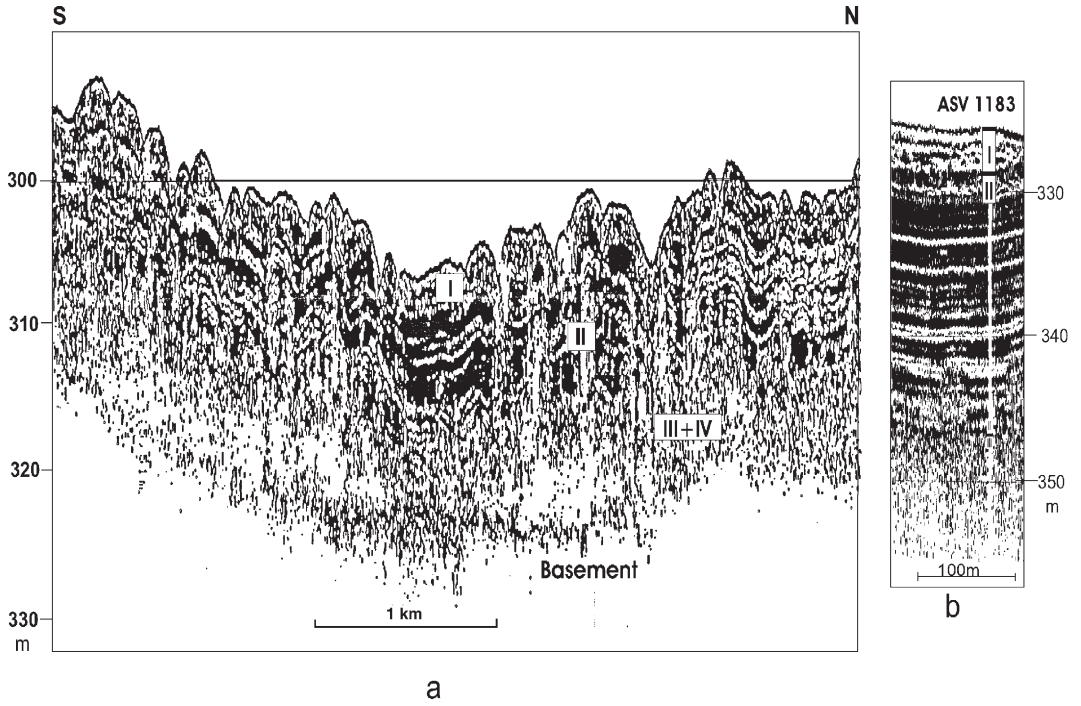

Fig. 10. *Parasound* seismic profile shot at the south-eastern margin of the Central Deep near ASV 1183 site (a) and during coring (b). The core penetrated upper transparent layer corresponding to Unit I, and recovered the uppermost semi-transparent bed of the underlying thick strongly stratified seismic unit which we interpret as an analogue of lithostratigraphic Unit II.

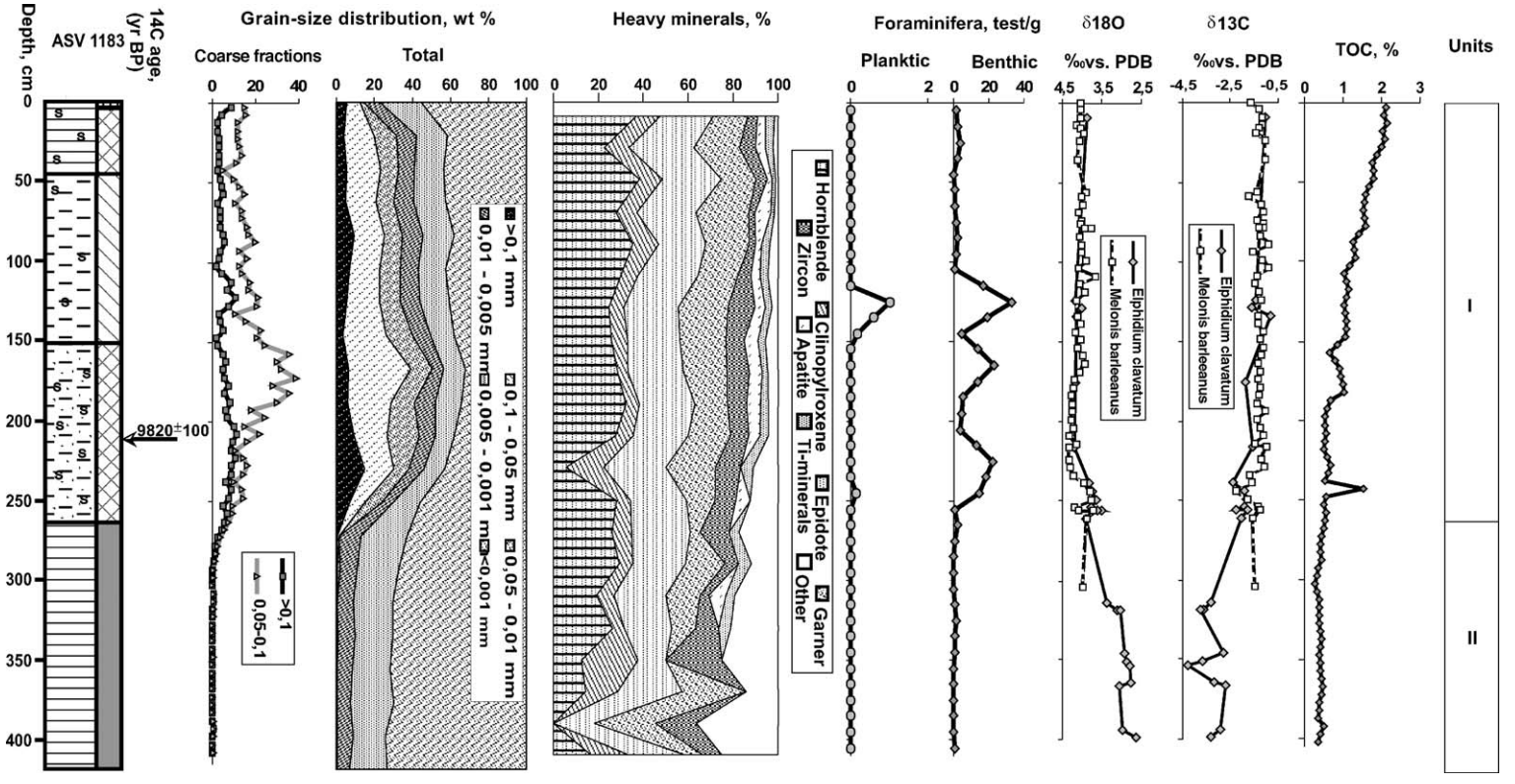

Fig. 11. Core ASV 1183 from the southern margin of the Central Deep (for location see Figs. 1 and 2) showing lithology of sediments, a ^{14}C date, distribution patterns of coarse fractions, total grain size, heavy minerals, planktic and benthic foraminiferal number, stable isotopes, and TOC. For lithological symbols, see Fig. 6.

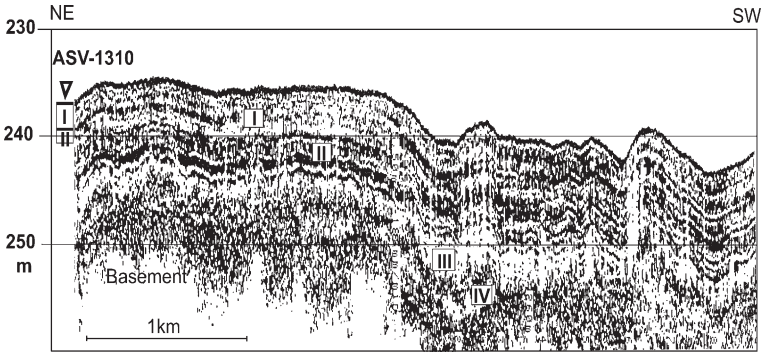

Fig. 12. *Parasound* seismic profile shot immediately after leaving the ASV 1310 site in the Western Novaya Zemlya Trench. The core penetrated upper indistinctly stratified seismic layer corresponding to lithostratigraphic Unit I and recovered below a sand layer likely displayed as a strong reflector in the stratified seismic pattern of Unit II.

eastern Franz Josef Land (core ASV 891), and the Sedov Trough (core ASV 897).

Turbidites also occur in Unit II. We found a 34 cm thick graded bed, with a distinct massive silty sand layer at the base and with laminated sandy silty clay above, in core ASV 1060 from the eastern slope of the Central Deep (Table 1, Fig. 1). Similar turbidites were also found in several cores from the northern Central Deep (Kalinenko, 1985).

5.1.4. Unit I: marine shelf depression facies (Holocene)

A distinct boundary commonly separates Units II and I. It is marked by simultaneous changes in color, sedimentary structures, grain size, physical properties, abundance of foraminiferal fauna, and organic matter content. A characteristic olive gray color, from light to dark olive gray and black due to the presence of diagenetic iron sulfide (hydrotroilite) replaces the yellowish and brownish shades of Unit II sediments at this boundary. An homogeneous structure, burrow mottling, and diffuse bedding expressed by uneven distribution of black hydrotroilite inclusions become the dominant features of the sediment, whereas lamination generally disappears. Most often, the sand content decreases (Figs. 6, 8 and 13), and only in core 1183 (Fig. 11) it increases. The abundance and diversity of foraminifers increase substantially and macrofaunal remains (bivalve shells, polychaeta tubes) appear sporadically above the Units II/I boundary. The TOC content increases and the contribution of marine organic matter derived from plankton production becomes dominant, constituting more than 80% of TOC (Romankevich et al., 2000).

In seismic records, the acoustically transparent upper layer corresponds either entirely to the Unit I (Figs. 7, 10 and 12), or to the sum of Units I+II, if the acoustic properties of both units are similar (Fig. 5).

As shown by seismic data (Figs. 5, 7, 10 and 12) and core records (Table 1 and Figs. 2–4), the thickness of Unit I varies from several decimeters to 5–6 m in shelf depressions, and it practically wedges out on submarine rises. Relatively thick (>2 m) Unit I sections are recovered from local hollows or valleys (e.g. cores ASV 880, ASV 883, ASV 1221, ASV 1183, ASV 1157; Figs. 2–4), whereas wide flat areas on depressions floor and local hills are commonly covered with a thin (less than 1 m) blanket of Unit I sediments (e.g. cores ASV 841, ASV 861, ASV 875, ASV 1190, ASV 1212; Table 1).

The Holocene age of Unit I is constrained by 23 AMS ^{14}C dates in 4 cores (Table 2). However, the Units II/I boundary is somewhat diachronous being younger in the north (ASV 880) and older in central (ASV 1200) and southern (ASV 1183) parts of the BS (Ivanova et al., 2002). Age models based on the AMS dates are published elsewhere (Duplessy et al., 2005). The linear interpolation between the dates suggests considerable variations in sedimentation rates during the Holocene, with maximum values (up to 74 cm/ka) obtained for the lowermost part of the Unit I in Core ASV 880 (Ivanova et al., 2002).

5.2. Characteristics of shelf depression facies

5.2.1. Grain-size distribution

The four lithostratigraphic units differ markedly by their grain size. They show generally a stepwise decreasing trend in the coarse fractions content with sharp changes at unit boundaries (Figs. 6, 8, 13 and 15). Only in Core ASV 1183 (Fig. 11), Holocene sediments are coarser than those of Unit II, which consists here of an extremely fine-grained clay. In several cores (e.g. ASV 880, ASV 1200, ASV 1157), the base of Unit I is slightly enriched in sand.

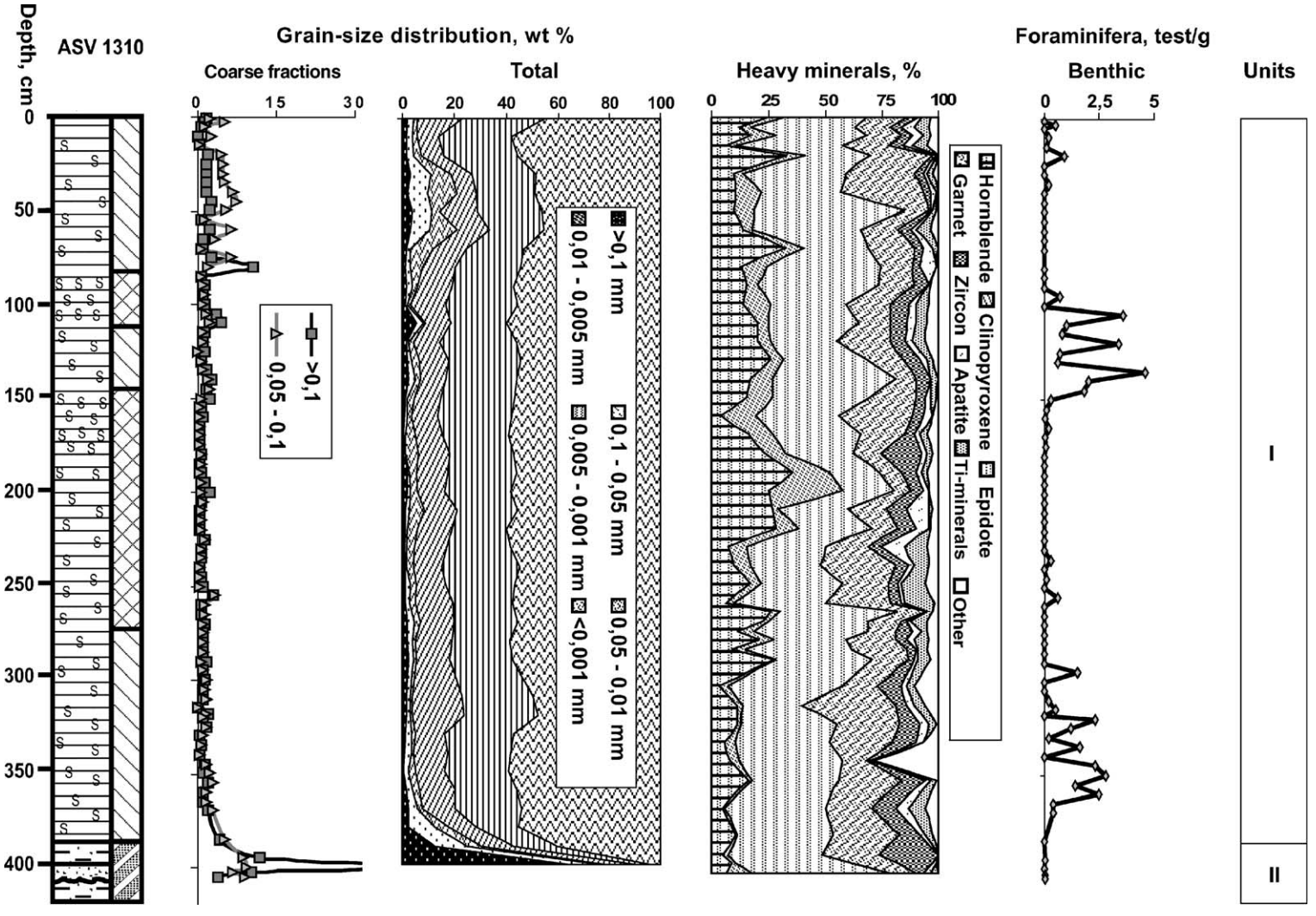

Fig. 13. Core ASV 1310 from the Western Novaya Zemlya Trench (for location see Figs. 1 and 4) showing lithology of sediments, distribution patterns of coarse fractions, total grain size, heavy minerals, and benthic foraminiferal number. For lithological symbols see Fig. 6.

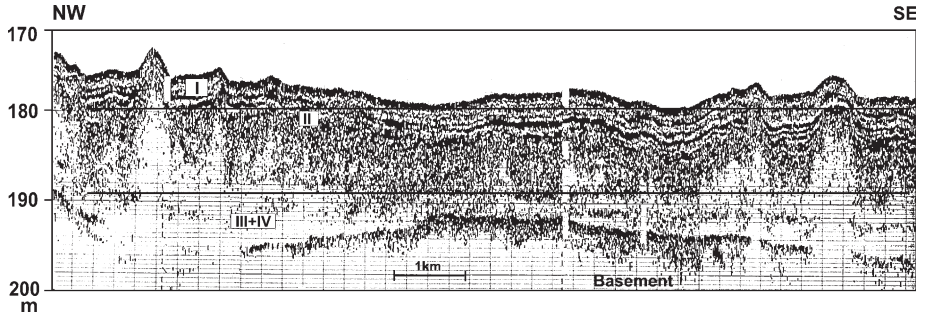

Fig. 14. *Parasound* seismic profile shot adjacent to the ASV 1157 site in the southern continuation of the Western Novaya Zemlya Trench (Fig. 1). We interpret the upper stratified unit above the strong reflector arbitrarily as the Holocene, based on dates in Core 1157 (see Fig. 15). The indistinctly stratified layer below this reflector likely represents Unit II, and the transparent basal unit above the basement, with its rugged surface topography, may consist of morainic deposits (?).

The comparison of grain-size distribution records (Figs. 6, 8, 9, 11, 13 and 15) suggests that variations in granulometry of the four units mainly result from changes in relative proportions of two major granulometric components: the generally uniform fine-grained material (<0.01 mm) and the coarse fractions (>0.05 mm). This bimodality in grain-size distribution spectra reflects the independent behavior of both components during sedimentation.

The pelite-size material (<0.01 mm), strongly dominated by finest clay (<0.001 mm), amounts more than 60% of total sediment in Unit III through Unit I (up to 98% of the Unit II sediment in core ASV 1183), hence pointing to a fine-grained nature of the post-glacial shelf depression facies. Coarser grain size, with the pelite content less than 30% characterizes the glacial till of Unit IV (Figs. 6 and 8) and the deglacial sand beds of Unit II in the Western Novaya Zemlya trench (Fig. 13).

The coarse sediment component (>0.05 mm) commonly consists of a granulometrically unsorted heterogeneous material characteristic for IRD. Coarse debris (gravel, pebbles) are common in Units IV and III, and rare in Units II and I, where the very fine sand (0.1–0.05 mm) constitutes a major proportion of the >0.05 mm fraction in some cases (e.g. in Unit I of core 1183, Fig. 11).

5.2.2. Heavy minerals

The composition of transparent terrigenous heavy minerals was studied in four cores from the western N–S transect (Figs. 6, 8, 9 and 11) and two cores from the eastern transect (Figs. 13 and 15). The six records exhibit considerable differences between mineral associations, both along the transects and between lithostratigraphic units.

Heavy minerals in core ASV 880 (Fig. 6) are dominated by clinopyroxene associated with epidote as a second-order mineral. Core ASV 1200 (Fig. 8) shows two diverse mineral associations. Garnet dominates in Units II–IV, with clinopyroxene and apatite as second-order components. The mineral association of Unit I sediments differs from that of underlying units by its higher epidote, clinopyroxene, and lower garnet, apatite contents. The garnet-dominated heavy mineral association, with rather high zircon and Ti-minerals content, is identified in Units III and IV(?) of core ASV 1190 (Fig. 9). Core ASV 1183 (Fig. 11) is characterized by garnet–epidote–hornblende association, with rather high zircon content at some levels, and with abundant mica (counted as "other") in Unit II.

Epidote, garnet, and hornblende are among dominant minerals in cores ASV 1310 (Fig. 13) and ASV 1157 (Fig. 15), whereas clinopyroxene is high in ASV 1157 and low in ASV 1310.

5.2.3. Clay minerals

Pilot X-ray diffraction analyses of the <0.001 mm fraction reveal relationships between the main clay minerals (illite, smectite, chlorite, and kaolinite) of the lithostratigraphic units (Table 3).

Most analyses of Unit III, as well as a single sample from Unit IV, show relatively low illite content (18–39%) and high chlorite+kaolinite values (52–75%), with smectite commonly below 10%.

Clay mineral associations in Unit II sediments are characterized by 22–50% of illite, 29–78% of chlorite+kaolinite, and 0–45% of smectite (Table 3). The higher smectite and lower chlorite+kaolinite values are found in the Unit II of core ASV 858 from the Persey trough suggesting a local smectite anomaly.

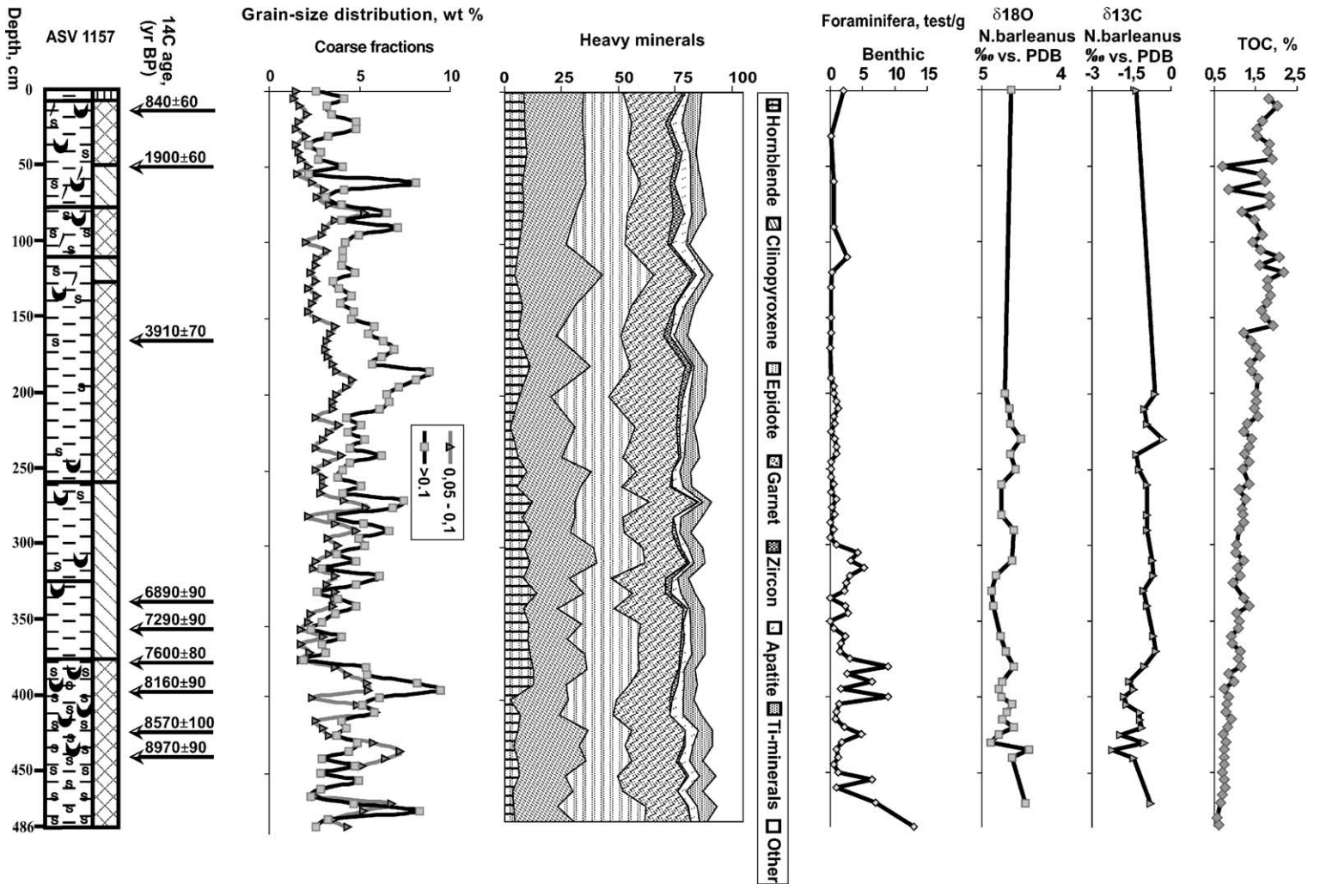

Fig. 15. Core ASV 1157 from the southern continuation of the Western Novaya Zemlya Trench (for location see Fig. 1) showing lithology of sediments, ^{14}C dates, distribution patterns of coarse fractions, heavy minerals, benthic foraminiferal number, stable isotopes, and TOC. For lithologic symbols see Fig. 6.

Table 3
Relative content of clay minerals in <0.001 mm fraction, % of sum

Station ASV no	Interval, (cm)	Relative content of clay minerals (%)					Unit
		Illite	Smectite	Chlorite	Kaolinite	Chlorite+kaolinite	
Western transect							
144 (880)*	0–3	22	30	26	22	48	I
	59–60	25	10	–	–	65	I
861	3–5	44	12	22	22	44	I
858	53–55	37	17	24	28	46	I
	63–65	32	16	25	27	52	I
	78–80	31	8	31	30	61	I
	93–95	27	19	26	28	54	II
	103–105	30	6	32	32	64	II
	0–2	28	43	14	15	29	I
	13–15	42	26	17	15	32	I
	155–157	47	12	20	21	41	I
	207–209	26	45	15	14	29	II
	257–259	26	22	25	27	52	III
	285–287	39	5	29	27	56	III
	330–332	35	1	36	28	64	III
1200	44–46	30	15	30	34	64	I
	189–191	28	9	32	31	63	I
	244–246	20	10	–	–	70	II
	304–305	18	7	–	–	74	III
	349–351	25	0	34	41	75	IV
841	8–10	36	28	18	18	36	I
	30–32	50	19	15	16	31	II
	100–102	57	4	20	19	39	III
	114–116	28	2	34	36	70	III
	119–120	28	8	30	33	63	III
Eastern transect							
1310	309–311	29	24	35	12	47	I
	349–351	34	6	45	15	60	I
	399–401	22	0	–	–	78	II
Russkaya Gavan'							
988	4–5	42	0	–	–	58	I
987	297–298	39	0	–	–	61	I
	582–583	42	5	–	–	53	I

*Core 144 is retreaved at site ASV 880.

The highest chlorite+kaolinite (78%) is detected in the laminated sand and mud present at the bottom of core ASV 1310 from the Western Novaya Zemlya trench.

In Unit I, the illite content varies within 22–47%. The proportion of chlorite+kaolinite among clay minerals varies from 29% to 65%, with almost equal values of both individual minerals. Some uppermost Holocene sediments are relatively enriched in smectite (up to 43% in core ASV 858). A specific association with maximum chlorite (35–45%) and low kaolinite (12–15%) occurs in the lower part of Unit I from the Western Novaya Zemlya trench (core ASV 1310).

5.2.4. Foraminifers

Diatoms, coccoliths, pteropods, ostracods, and small mollusks are very rare in BS postglacial sediments. More or less representative benthic (and occasionally planktic) foraminiferal assemblages characterize only specific Holocene (Unit I) depression facies (Tables 4 and 5).

Unit IV does not contain in situ microfossils. Only several probably reworked tests of *Neogloboquadrina pachyderma* sin. are found in the ASV 880 core catcher sample.

Unit III sediments contain rare foraminifers consisting of Pleistocene and reworked Mesozoic benthic species, mainly agglutinated (Table 4). Tests of

Table 4
Benthic foraminiferal assemblages

Unit	Western transect (without Core ASV 880)	Northern transect (including Core ASV 880)	Eastern transect
IV	Barren	Barren	Unit not recovered
III	Generally barren, Very rare *Elphidium* spp., *C. reniforme*, *I. helenae/norcrossi*, *M. barleeanus*	Generally barren, very rare *Elphidium* spp., *C. reniforme*, *I. helenae/norcrossi*, *M. barleeanus*	Generally barren, very rare *Elphidium* spp., *C. reniforme*, *E. clavatum*, *M. barleeanus*, *E. bartletti*, *E. subarcticum* *I. norcrossi,*, *Buccella* spp.; and very rare *Bul. marginata (likely reworked)*
II	Generally barren, rare *E. clavatum*, *C. reniforme*, *I. helenae/norcrossi*, *M. barleeanus*, and 11 very rare species	Generally barren, in **Core ASV 880**: very rare *E. clavatum*, *C. reniforme*, and 'atlantic' species: *C. teretis*, *Cib. wuellerstorfi*, *P. bulloides,*	Barren with few levels in **Core ASV 902** containing *Cib. lobatulus* and some other very rare species
I	Dominant species in **cores ASV 1200**, **ASV 1221**, **ASV 858**, **ASV 841**, **ASV 1183**: *E. clavatum*, *C. reniforme*, *M. barleeanus*, common species: *I. norcrossi*, *Buccella* spp., *E. subarcticum*, *N. labradoricum*, *Cib. lobatulus*, rare species: *I. helenae*, *E. incertum*, *E. bartletti*, *T. fluens*, *H. orbiculare*, *V. loeblichi*, *C. eretis*, *A. gallowayi*, *Quinqueloculina* sp., *P. williamsoni*, *Ad.glomerata*, *Reophax* spp., *Por. karika*, and about 15 very rare species. Most samples are barren in **cores ASV 861**, **ASV 1190**, **ASV 1213** and **ASV 1217**, few samples contain the species pointed above.	Most samples are barren or almost barren in cores **ASV 875** and **ASV 877.** Dominant species in **Core ASV 880 (**and also in few samples from **Core ASV 883** and from the upper 15 cm of **Core ASV 891):** *E. clavatum*, *C. reniforme;* common species: *Buccella* spp., *I. norcrossi*, *M. barleeanus*, *E. subarcticum*, *N. labradoricum*, *I. helenae* (especially abundant in the middle part of the unit in Core ASV 880); rare species: *E. incertum*, *M. barleeanus*, *C. teretis*, *Cib. lobatulus*, *V. loeblichi*, *Por. karika*, and about 15 very rare species.	Most samples are barren or almost barren in cores **ASV 891** and **ASV 1006.** Common species in **Core ASV 902** and in the upper 72 cm of **Core ASV 897**: *C. reniforme*, *E. clavatum*, *I. norcrossi*, *M. barleeanus*, *E. subarcticum*, *N. labradoricum*, *I. helenae*, *Cib. lobatulus*, *B. tenerrima*, *B. frigida*, *C. teretis*; and about 10 very rare species Common species in **Core ASV 1310:** *C. reniforme*, *Buccella* spp., *E. clavatum*, *N. labradoricum*, *H. orbiculare;* rare species: *P. williamsoni*, *C. teretis*, *E. bartletti*. Arenaceous species: *Cr. Subglobosum* , *Labrospira* sp., *R. Contortus*, *Troc. nana*, *S. biformis*, *Troch. bullata* predominate in the upper 90 cm. Common species in the lower and middle parts of **Core ASV 1157**: *C. reniforme*, *E. clavatum*, *H. orbiculare*, *N. labradoricum*, (and *Al. crassimargo* at 375 cm), rare species: *P. williamsoni*, very rare species of genera *Reopax*, *Recurvoides*, *Rhabdammina*, *Cribrostomoides;* highly diverse but poorly preserved assemblages, mainly represented by the same arenaceous genera, especially by species *S. biformis*, are found in the upper 110 cm.

Genera names: *C.*=*Cassidulina*, *I.*=, *Islandiella*, *M.*=*Melonis*, *E.*=*Elphidium*, *E. clavatum*=*E. excavatum* forma *clavata*, *P.*=*Pullenia*, *Cib.*=*Cibicides*, *N.*=*Nonion*, *H.*=*Haynesina*, *T.*=*Trifarina*, *V.*=*Virgulina*, *A.*=*Astrononion*, *Bul.*=*Bulimina*, *P.*=*Pyrgo*, *Cyc.*=*Cyclogyra*, *Tril.*=*Triloculina*, *Por.*=*Portatrochammina*, *Ad.*=*Adercotryma*, *S.*=*Spiroplectammina*, *Al.*=*Alveolophragmium*, *Cr.*=*Crisrostomoides*, *R.*=*Recurvoides*, *Troc.*=*Trochammina*, *Troch.*=*Trochaminella*.

Mesozoic foraminifers bear iron oxide films and are rounded indicating reworking. Rather good preservation of Pleistocene calcareous tests, as well as a presence of a few well-preserved aragonite shells of pteropod species *Limacina helicina* in core ASV 858 point to their in situ burial.

Unit II sediments in all cores from the western transect (Fig. 2) contain rare reworked Mesozoic foraminifers and ostracods. The benthic foraminiferal fauna is more diverse in Unit II than in Unit III, especially in core ASV 880 (Table 4). However, the foraminiferal abundance is still extremely low, generally <0.05 tests/g, with maximum values up to 0.8–1.4 tests/g at some levels in Core ASV 1183, and many samples are barren. The most abundant and diverse assemblage dominated by *Elphidium excavatum* forma *clavatum* and *Cassidulina reniforme* is recorded in one sample of core ASV 1200.

Unit I is characterized by much more abundant and diverse fossil fauna. Macrofossils are represented by rare molluscs, sponge spicules, and locally abundant polychaeta tubes, while microfossils include ostracods, foraminifers and very rare diatoms (only in the upper layer). Calcareous foraminifers strongly predominate

Table 5
Planktic foraminiferal assemblages

Unit	Western transect (without Core ASV 880)	Northern transect (incl. Core ASV 880)	Eastern transect
IV	Barren	Very rare *N. pachyderma* sin. (likely reworked)	Unit not recovered
III	Rare *N. pachyderma* sin	rare *N. pachyderma* sin	Barren
II	Generally barren, rare *N. pachyderma* and *T. quinqueloba*	Generally barren, in **Core ASV 880**: rare *N. pachyderma* sin. and *T. quinqueloba*	Barren
I	Generally barren, rare *N. pachyderma* sin., very rare *T. quinqueloba* and *N. pachyderma* dex.	Generally barren, in **Core ASV 880**: rare *N. pachyderma* sin., very rare *T. quinqueloba* and *N. pachyderma* dex.	Generally barren, rare *N. pachyderma* sin. and *N. pachyderma* dex.only in **cores ASV 897** and **ASV 902**

Genera names: *T.* = *Turborotalita*, *N.* = *Neogloboquadrina*.

over agglutinated ones in benthic assemblages. The preservation varies considerably, and dissolution is especially extensive in the south-eastern part of the BS (cores ASV 1183, ASV 1157, ASV 1310).

Planktic foraminifers are generally scarce and are mainly represented by the polar species *N. pachyderma* sin. Extremely rare boreal species *N. pachyderma* dextral and *Turborotalita quinqueloba* occur sporadically (Table 5).

In the western transect (Fig. 2), the abundance of benthic foraminifers varies within 0.3–41 tests/g in cores ASV 1183 (Fig. 11), ASV 1200 (Fig. 8), ASV 858, and up to 63 tests/g in ASV 880 (Fig. 6). Benthic foraminiferal assemblages demonstrate pronounced lateral and temporal variability including changes in species dominance (Duplessy et al., 2001; Ivanova, 1999, 2002). The number of species per sample ranges from 7–24 in the northernmost core ASV 880 to 14–27 species in the central part of the BS (cores ASV 858 and ASV 1200 from the Persey Trough). The most diverse assemblages, but at a low abundance level, are found in the southernmost core ASV 1183, where many tests are etched by dissolution. Similar highly diverse assemblages are typical for the south-western Barents Sea (Hald et al., 1989, 1990).

In the northern and eastern transects (Figs. 3 and 4), most samples of Unit I are barren or contain rare foraminiferal tests (Tables 4 and 5). Rather abundant and diverse benthic foraminiferal assemblages occur at some levels in cores ASV 883, ASV 891, ASV 897, ASV 902 from the northern BS, and in cores ASV 1310 (Fig. 13), ASV 1006, ASV 1157 (Fig. 15) from the south-eastern BS. Benthic foraminiferal assemblages of the northern BS are strongly dominated by *E. clavatum* and *C. reniforme*, whereas, their content is similar to that of some other species in Holocene assemblages from the south-eastern BS (Table 4). In cores ASV 1310 and ASV 1157, *Nonion labradoricum* is a common species of the diverse assemblages (along with *Haynesina orbiculare* in ASV 1157). Poorly preserved rare calcareous tests indicate a strong dissolution, and agglutinated species predominate in the assemblages from the upper intervals of Unit I in these cores.

5.2.5. Stable isotopes

Oxygen and carbon isotopes in benthic foraminiferal tests have been measured in cores ASV 880 (Fig. 6), ASV 1200 (Fig. 8), ASV 1183 (Fig. 11) and ASV 1157 (Fig. 15). Isotopic records of planktic species *N. pachyderma* sin. have been obtained only in cores ASV 880 and ASV 1200. Small variations in the $\delta^{18}O$ records (<1‰) reflect changes in both BS water temperature and isotopic composition. The isotopic records of benthic foraminifers for Unit II obtained only in Core ASV 1183 (Fig. 11) demonstrate upward increasing trends of $\delta^{18}O$ and $\delta^{13}C$ suggesting a decrease in glacier meltwater contribution to the bottom water. The records for Unit I (Figs. 6, 8, 11 and 15) show small, but significant variations, which cannot be directly correlated between the cores. The paleoceanographic implications of the stable isotope measurements are discussed elsewhere (Duplessy et al., 2001, 2005).

5.3. Facies of submarine rises

Summits of submarine rises in the open BS represent typical non-depositional and erosion environments. The shallower ones, with depth <100 m, are practically sediment-barren. Bedrock outcrops occupy most bottom surface, and only small patches of sand and gravel, as well as rare shell accumulations occur locally. Nearshore shoals are mainly covered with sand (e.g. Gurevich, 1995; Levitan et al., 2003a).

On deeper rise summits, thin discontinuous muddy sand lenses alternate with moraine and bedrock outcrops. Our grab samples from Murmansk, Central, and Persey rises consist of boulders, pebbles, ferruginous nodules, mollusk and balanus shells mixed with mud and muddy sand. In some cases, a semi-liquid brown mud covers pebbles with attached alive hydroids and

other epifauna, thus indicating the unstable character of the mud. It settles during still water and is washed off when current velocity increases. The coarse material accumulates as IRD or products of moraine erosion, and concentrates as a residual deposit by removal of fine fractions.

6. Discussion

The studied core sections from shelf depressions display a successive sedimentary cycle from glacial till facies of the LGM through proximal and distal glaciomarine facies of the deglaciation to specific recent marine facies reflecting present Arctic shelf environments.

6.1. Sedimentation processes

The studied cores from eastern BS shelf depressions recovered fine-grained, clay-dominated terrigenous sediments of the last deglaciation and Holocene (Units III–I) overlying unsorted coarse-grained basal glacial till (Unit IV). Variations in thicknesses of the lithostratigraphic units I–III (Table 1, Figs. 2–4) are essentially determined by mass accumulation rates of the fine-grained component (clay and silt). The coarse fractions constitute a minor admixture in the fine-grained mud from shelf depressions. Deposition of sand laminae, lenses and even relatively thick sand interbeds of the Unit II (as those in core ASV 1310, Fig. 13), or assumed debris flow deposits of the Unit III, contribute much less material to the total sediment budget of the post-glacial BS than accumulation of the fine-grained component. Thin discontinuous beds of sand and coarser material on submarine rises represent residual IRD facies (after removal of fine-grained material by bottom currents), and their contribution to the sediment budget of the BS is negligible.

Ternary diagrams of three pelite (<0.01 mm) fractions (Fig. 16) show that the analytical results for Units I–III fall into a rather narrow area close to the finest clay fraction (<0.001 mm) corner. Fine-grained matrix of the glacial till at the base of cores ASV 880 (Fig. 6) and ASV 1200 (Fig. 8) demonstrates similar relationship at a much lower level of pelite content. Such grain-size pattern is best explained in terms of a single fine-grained component source, which is most likely the glacier meltwater discharge that apparently dominated during deglaciation. Somewhat coarser composition of the pelite fraction in Holocene sediments (Unit I) suggests a contribution of other fine-grained sediment sources, such as coastal wave erosion and permafrost destruction, river runoff, and sea ice rafting.

At present, the glacier meltwater discharge may contribute to more than 50% of the total fine-grained suspended sediment input into the BS (Medvedev and Potekhina, 1990), but a large part is captured in silled bays where glaciers discharge (Aibulatov et al., 1999). This is well illustrated by the core ASV 987 raised from the Russkaya Gavan' fjord, north-western Novaya Zemlya (Fig. 1). The sediments are totally derived from the Shokalski glacier meltwater discharge. They are characterized by a dominant clay content that constitutes 70–80% of the total sediment. The mud accumulates with an average rate of 6 mm/yr during the last 800 yr (Murdmaa et al., 2004). This example shows the potential of glacier meltwater discharge as a fine-grained sediment source for present-day conditions.

Meltwater discharge should have been stronger during the deglaciation, when ice sheets intensely melted, draining directly into the open sea. Amounts of sediment released from the ice depended on ice sheets volume and melting rates (i.e. on summer temperatures and duration). Thick Unit II sediments in the south-eastern BS (e.g. Polyak et al., 1995; Polyak and Mikhailov, 1996; Gataullin et al., 2001), also exemplified by our data (Figs. 10 and 11), possibly indicate more abundant meltwater discharge from the intensely melting large ice sheets during warmer and longer

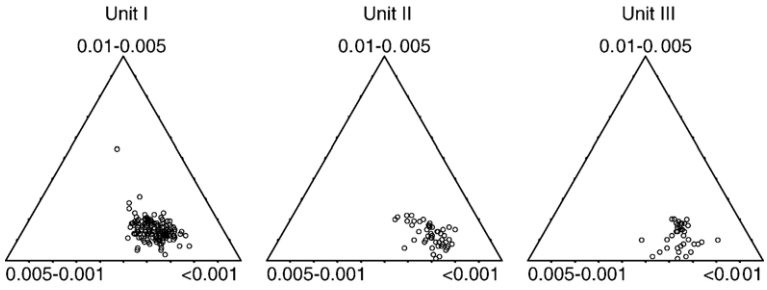

Fig. 16. Ternary diagrams showing relationship between grain-size fractions 0.01–0.005 mm, 0.005–0.001 mm and <0.001 mm in lithostratigraphic units I, II, and III.

summer seasons, as compared to the northern BS (e.g. ASV 880).

Available data on clay mineralogy of surface sediments from the Arctic Ocean and its Eurasian shelf (Stein et al., 1994; Gurevich, 1995; Nürnberg et al., 1995; Shelekhova, 1998; Wahsner et al., 1999; Kalinenko, 2001; Levitan et al., 2003a; Viscosi-Shirley et al., 2003) show an illite-dominated background, with chlorite as a second-order mineral and low smectite, except for Kara and Chukchi seas, where high smectite contents are recorded. The chlorite-illite assemblage mainly originates from Siberian rivers discharge. Local kaolinite anomalies are noted in the St. Anna Trough (Levitan et al., 1999), and in the central Barents Sea (Wright, 1974; Gurevich, 1995; Wahsner et al., 1999).

Our data on clay mineralogy of post-glacial sediments reveal a dominant illite–chlorite–kaolinite association with low smectite content (Table 3). Higher chlorite+kaolinite and lower illite content in deglacial sediments, as compared to the Holocene unit, and especially the kaolinite maximum in glacial till from the Persey Trough (ASV 1200) suggest a glacier meltwater source for these minerals. Similar dominant chlorite+kaolinite association was also found in the Russkaya Gavan' fjord sediment derived from the modern glacier meltwater load (Table 3, Murdmaa et al., 2004). Hence, the above mentioned 'kaolinite anomalies' in surface sediments of the central BS and St. Anna Trough might result from local reworking of moraine deposits primarily enriched in kaolinite due to bedrock glacial erosion.

Therefore, both clay mineralogy and grain-size patterns of the fine-grained component of sediments support the hypothesis that at least during the deglaciation, it originates mainly from the glacier meltwater discharge. In the Holocene, small glaciers on the northern archipelagoes could not supply enough clay to maintain the accumulation rates observed over the BS, and the remote riverine sources marked by high illite content became significant especially in the southern BS and Pechora Sea (Levitan et al., 2003a).

Precipitation of aerosol contributes only to a minor proportion of the fine-grained component budget in modern sedimentation (Shevchenko, 2003). However, this proportion might have increased, when the aeolian dust accumulated over a long period of the Late Weichselian ice sheet growth, and was subsequently released by rapidly melting glaciers during deglaciation. The clay mineralogy of modern aerosols supports this suggestion. According to Shevchenko (2003), illite and chlorite+kaolinite dominate in the clay mineral assemblage of aerosols collected over the Kara and Barents seas, whereas smectite content is low. The illite–chlorite–kaolinite aerosol assemblage is similar to those of deglacial units III and II (e.g. ASV 1200) and of recent sediments from the Russkaya Gavan' fjord.

Present direct river discharge into the BS is negligible, and only a minor part of suspended matter delivered by Pechora, and Severnaya Dvina might contribute to the clay fraction budget via the Pechora, and White seas respectively in the Holocene. During the deglaciation, and especially its final phase, maximum riverine discharge has been recorded in the Kara Sea (e.g. Stein et al., 2004), as well as in the Laptev Sea (e.g. Spielhagen et al., 2005). Sediment delivery from the Pechora River possibly also increased, as it discharged closer to the deep BS basin due to lower glacioeustatic sea level. This riverine material might contribute to the accumulation of the thick Unit 2 sequence in the south-eastern BS.

As it is widely discussed, sea-ice rafting plays a major role among the primary factors of fine-grained sediment delivery to the Arctic Ocean and Eurasian Arctic seas including the BS (e.g. Elverhoi et al., 1989 and many later publications). We agree that pack ice from the Transpolar Drift may contribute a considerable proportion of clay to the suspended matter budget of the BS, especially in the Holocene. However, there is no evidence of the ice-rafted suspension settling neither in clay mineralogy of surface sediments, nor in Unit I thickness within the seasonal sea-ice zone, where the 'turbid' pack ice melts.

All products of glacial scouring accumulate together as basal till beneath the grounded ice sheet and outlet glaciers (e.g. Unit IV in ASV 880), but a primary fractionation of the fine-grained suspension from coarse debris occurs already in subglacial underflows. Turbid meltwater plumes at the glacier front resulting in abundant suspension settling (e.g. Dowdeswell and Drewry, 1989; Ó Cofaigh and Dowdeswell, 2001) possibly contributed to the fine-grained sediment deposition in the glacier-proximal environments of the open BS during the initial deglaciation stage. As shown by Dowdeswell and Cromack (1991), such plumes can transport material up to fine sand size. The mud accumulation from turbid meltwater plumes combined with iceberg rafted coarse debris deposition likely result in massive proximal glaciomarine diamict facies of Unit III recovered by most of our cores. Unit III may also comprise iceberg-turbated till facies described from various Arctic regions (e.g. Hald et al., 1990; Dowdeswell et al., 1994). Horizontal coarse debris interbeds in Unit III sediments (e.g. ASV 858, ASV 883, ASV 891)

suggest episodic deposition from debris flows in some local depressions.

Further fractionation of the fine-grained suspension supplied by glacier meltwater from the coarse glaciogenic material occurs during the main phase of deglaciation. Lack of dropstones in most laminated Unit II sediments from the open BS is evidence of suppressed iceberg rafting. Meanwhile, fine sand is involved into sediment transport by gravity flows and bottom currents resulting in formation of sand laminae and lenses in laminated Unit II sequences (e.g. ASV 880).

We interpret the laminated sediments of Unit II as deposits of various glaciomarine gravity flows. However, the thick strongly stratified seismic unit from the southeastern BS (e.g. Polyak et al., 1995; Gataullin et al., 2001) provides some evidence of suspension settling from above mentioned turbid glacier meltwater plumes: such as a blanket-like undulating geometry of strata and extremely fine grain-size of mud members, the upper of which is recovered by core ASV 1183 and a meltwater signature of the oxygen isotope composition (Figs. 10 and 11). Sand members of the stratified seismic facies exemplified by Unit II in core ASV 1310 (Fig. 13) may represent glaciomarine sandy turbidites (e.g. Ó Cofaigh and Dowdeswell, 2001).

Thinly laminated, fine-grained, variegated (brown and gray) sequences from the Persey Trough (e.g. ASV 858, ASV 1200) and some other locations presumably represent rhythmic suspension flow deposits. It is shown that a fine-grained sediment concentration >30 g/l of glacier meltwater is necessary to create a gravity-driven near-bottom suspension flow in a glaciomarine environment (Gilbert, 1983). Similar gravity flows, but with higher suspension concentration due to more abundant glacier meltwater discharge, possibly deposited silty mud with fine sand laminae (e.g. ASV 880). A relatively coarse-grained dark gray interbed within the laminated Unit II interval in core ASV 1200, similar to Unit III sediments, likely represents a debris flow deposit related to a readvance of the glacier front. Turbidites found at the base of Central deep slope (ASV 1060, as well as those described by Kalinenko, 1985) indicate turbidity currents activity at the end of deglaciation, when the glacier front retreated to the Admiralty Bank line (Gataullin et al., 2001).

Today, the fine-grained sediments distribute over the BS within surface (above the pycnocline) and near-bottom nepheloid layers. The concentration of suspended matter in the surface layer shows an almost even distribution in the open sea, but is considerably higher near outlet glaciers, small river mouths, and pathways of more turbid waters flowing from the White Sea and Kara Sea (Aibulatov et al., 1999). The near-bottom nepheloid layer covers rise slopes and occasionally demonstrates a higher suspension concentration at the slope base. However, suspension concentration in the nepheloid layer is by several orders of magnitude lower than that necessary for initiation of gravity flows resulting in deposition of laminated sequences characteristic for Unit II. This suggests a low-density slow nepheloid flow mechanism that possibly redistributes suspended fine-grained material from submarine rises to local depressions, where enhanced clay accumulation rates are detected in studied cores during the Holocene. Sea ice freezing brine cascades responsible for saline and cold bottom water formation in shelf depressions (e.g. Midttun, 1985; Ivanov and Shapiro, 2005) may promote the low-velocity nepheloid flows throughout the seasonal sea-ice zone.

Iceberg and sea-ice rafting constitutes the main mechanism of coarse fraction transport in the modern BS, but its accumulation rates are extremely low, as compared to those of the fine-grained material in shelf depressions during the Holocene. This follows from the very low coarse fractions content (commonly less than 10%) in Holocene sediments of the studied cores. The IRD concentrates on submarine rise summits as residual coarse-grained sediment facies due to removal of fine fractions by bottom currents, and maintains negligible sedimentation rates there.

However, a part of the finest sand (0.1–0.05 mm) is transported by bottom currents, brine-induced nepheloid flows, and even surface currents, as a minor constituent of suspended matter. Domination of the finest sand fraction (0.1–0.05 mm) over other coarse fractions in the lower Holocene interval of the Unit I in core ASV 1183 (Fig. 11) indicates sand sorting during the sediment transport, whereas IRD commonly consists of unsorted material.

Variations in heavy mineral associations demonstrate a relative contribution of the Franz Josef Land (FJL), Northern and Southern Novaya Zemlya (NZ), northeastern Russian plain (RP), and Kola Peninsula (KP) provenances to the 0.1–0.05 mm fraction budget. Along the western transect (Fig. 2), a southward decrease in clinopyroxene content (highest in ASV 880) and a relative increase in garnet, apatite, Ti-minerals, and zircon (ASV 1190, ASV 1200) reflects, in general, an interplay between contribution of FJL basalts and continental KP provenance. We suggest that the high-garnet association of Units II–III in cores ASV 1200 and ASV 1190 is directly derived from reworking of glacial

till (Figs. 8 and 9) which was transported by glacier ice from the KP provenance. The garnet–epidote–clinopyroxene association of Holocene sediments in the Persey Trough (ASV 1200) characterizes an integrated province of the central Barents Sea likely formed as a result of sea-ice rafting (mainly from FJL), suspended matter transport by surface currents (from different provenances), and reworking of earlier glacial or glaciomarine sediments on adjacent rises. Garnet, epidote, and hornblende, representing characteristic heavy minerals in Units II and I sediments of the south-eastern BS (ASV 1310, ASV 1157, ASV 1183), are likely derived from the nearby NZ and RP provenances (Levitan et al., 2003a).

6.2. Evolution of the facies system

Lithostratigraphic units from IV to I are commonly separated from each other by distinct facies boundaries, which reflect substantial environmental changes further discussed in this chapter.

6.2.1. The last glaciation (Unit IV)

Previous seismic and drilling data show that glacial erosion, glaciotectonic bedrock deformation, basal glacial till (bottom moraine) deposition, and its overconsolidation by the grounded ice sheet load characterize subglacial paleoenvironments in the BS during the LGM. Moraine ridges and mounds, both exposed and buried, are recorded by seismic profiling throughout the shelf (e.g. Gataullin and Polyak, 1997; Gataullin et al., 2001; Pavlidis et al., 2001, 2005; see also Figs. 5 and 7). However, many of those are formed in a marine environment at retreating ice sheet margins by direct glacier discharge as proximal glaciomarine deposits during the deglaciation. Core ASV 880 (Figs. 5 and 6) likely recovered bottom moraine (Unit IV) of the outlet glacier that moved through the Franz Victoria Trough. The continental glacial origin of the diamicton (till) is inferred from the very low pore water salinity (Murdmaa et al., 1998; Bogdanov et al., 2001), the coarse-grained unsorted nature of the sediment, seldom orientation of rock clasts, and absence of in situ marine microfossils. We assume that similar stiff diamicton recovered from the Central Deep (ASV 1190), the Persey Trough (ASV 1221) and the Sedov Trough (ASV 897) also represent basal glacial till. Partial ice sheet melting from below likely resulted in a subglacial hydrological system (e.g. Ó Cofaigh and Dowdeswell, 2001) that provided fresh pore water and fine-grained matrix to the basal till.

6.2.2. Initial deglaciation stage (Unit III)

We suggest a glaciomarine origin for this unit, based on the dominant fine-grained fraction in the sediments, the pore water salinity close to that of seawater, although somewhat freshened (Murdmaa et al., 1998; Murdmaa and Ivanova, 1999; Bogdanov et al., 2001), the scarce occurrence of well preserved tests of extant benthic and planktic foraminifers (Tables 4 and 5) and rare findings of fresh-looking pteropod shells (Ivanova et al., 2002). Meanwhile, meltwater flows and icebergs could bring reworked Mesozoic foraminifera into the sediments, together with other products of bedrock glacial erosion (Murdmaa and Ivanova, 1999; Ivanova and Murdmaa, 2001; Pavlidis et al., 2001).

The initial deglaciation likely started by the detachment of the ice sheet from the sea bottom and the penetration of sea water into the deep troughs beneath the glacier ice that resulted in intense iceberg calving. The timing of this event is still unclear, because radiocarbon dating of Unit III is impossible. The data on IRD distribution and isotopic meltwater signals from the continental slopes of the BS indicate that the ice sheet began receding before 15 ka, or perhaps 16 ka (Svendsen et al., 2004b). The end of the initial deglaciation stage is constrained by the earliest ^{14}C dates of about 13.3 ka BP at the base of Unit II (Hald et al., 1990; Lubinski et al., 1996, 2001; Polyak et al., 1997). However, younger dates (<13 ka BP) are obtained from the south-eastern BS for "marine sediments above the till (minimum age of deglaciation)" (Svendsen et al., 2004b, p. 2; Fig. 1). We believe that an upper layer of the till was likely deposited in a proximal glaciomarine environment during the initial deglaciation, as our Unit III. Even younger Unit III sediments may occur near the Admiralty Bank line, possibly representing a Younger Dryas end moraine (Svendsen et al., 2004b). We speculated previously (Murdmaa and Ivanova, 1999) that the deglaciation of the BS began almost simultaneously with that of the Nordic seas, dated at about 15 ^{14}C ka BP (e.g. Hald et al., 1996), as a response to high latitude insolation increase and to sea level rise at ~16.5–16 ^{14}C ka BP (Lambeck et al., 2000). This corresponds to the model by Elverhoi et al. (1993) for the southern BS. A meltwater outflow from the Barents Sea into the Norwegian Sea and the Heinrich-1 event in the North Atlantic occurred at the same time (Sarnthein et al., 1995, 2000). This scenario is consistent with the suggestion of rapid disintegration of the marine-based BS ice sheet about 14.5– 13.5 ^{14}C ka (Jones and Keigwin, 1988; Lehman, 1991; Weinelt et al., 1991). Lubinski et al. (2001) also assume that the deglaciation started at about 15 ^{14}C ka BP in the outer

parts of Franz Victoria and St. Anna troughs. The last major meltwater outflow from the northern BS to the Arctic Ocean at about 15 ka BP that coincides with the rapid decrease in total ice volume of the Late Weichselian Eurasian ice sheet, is demonstrated by Svendsen et al. (2004a,b).

The depositional environment in the study area at the beginning of the deglaciation was characterized by the rapid destruction and retreat of the ice sheet from shelf depressions accompanied by intense iceberg calving and meltwater discharge. The proximal glaciomarine diamicton of Unit III accumulated on the top of the continental morainic deposits in the shelf depressions and on rise slopes, with bimodal grain-size distribution, saline pore water, and rare marine microfossils. It comprises submarine moraine ridge facies accumulated at the retreating glacier front, as recorded by seismic profiling (e.g. Gataullin and Polyak, 1997; Pavlidis et al., 2001); proper glaciomarine facies (massive diamicton) composed of a mixture of iceberg rafted debris with fine-grained glacier meltwater load, and gravity flow deposits (see Section 6.2.2).

Summits of submarine rises were still ice-capped, and served as local glacial material sources. We suggest that the garnet-dominated heavy mineral association of Units III and IV in cores ASV 1190 (Fig. 9) and ASV 1200 (Fig. 8) indicates a material delivery from the Kola Peninsula provenance to the central BS by the glacier ice, with subsequent local moraine reworking, possibly by iceberg turbation mechanism (Dowdeswell et al., 1994; Ó Cofaigh and Dowdeswell, 2001) during the initial deglaciation stage.

6.2.3. The main deglaciation stage (Unit II)

It began about 13 ^{14}C ka BP according to AMS datings near the base of the laminated unit corresponding to our Unit II, in several cores (Lubinski et al., 1996; Polyak and Mikhailov, 1996), or possibly earlier in the St. Anna Trough (Lubinski et al., 2001). A distinct facies change marks the transition from Unit III to Unit II. Many authors interpret this sharp boundary as the replacement of glacial diamicton by glaciomarine facies (e.g. Vorren et al., 1983, 1984; Gataullin et al., 1993; Lubinski et al., 1996, 2001; Polyak and Mikhailov, 1996). Our data show that this boundary likely reflects the transition from proximal to distal glaciomarine facies in the open BS.

The facies change at the boundary between Units III and II is expressed by a sharp decrease in IRD content, the development of lamination instead of a massive structure of Unit III, and common occurrence of brownish or yellowish color shades pointing to suboxic early diagenesis. These changes presumably reflect the cessation of intense iceberg calving owing to the retreat of ice sheets to archipelagoes and continental land, or blocking of icebergs by permanent pack ice (Dowdeswell et al., 2000), and the development of downslope suspension flows, which derived their fine-grained sediment load from intensely melting glaciers. Turbid meltwater overflows (e.g. Ó Cofaigh and Dowdeswell, 2001) might also contribute to the accumulation of thick laminated Unit II sediments from depressions of the southeastern BS. A considerable amount of fine-grained sediments may have been derived from wave and current erosion of Pechora Sea and Kanin Bank shoals, or from the Pechora River discharge, during a lower sea level stand (Gataullin et al., 2001). However, the heavy mineral association in Unit II sediments of core ASV 1183 assumes a possible material supply from the melting Novaya Zemlya ice sheet.

Meltwater discharge became a major sedimentary material source into the widened marine basin filled with freshened sea water. The freshening affected bottom water, as shown by the low pore water salinity (Murdmaa et al., 1998; Bogdanov et al., 2001) and light delta ^{18}O values of benthic foraminifers (Fig. 11; see also Lubinski et al., 1996, 2001).

Pulsed sedimentation strongly dominated during the main deglaciation phase as inferred by the widespread distribution of laminated and stratified sediments deposited by various gravity flows (see Section 6.1).

Severe sea-ice conditions during the deglaciation likely hindered biological productivity resulting in commonly rare occurrence of the foraminiferal fauna (Tables 4 and 5). Furthermore, the pulsed sedimentation prevented macro-and microbenthos to develop. Korsun and Hald (1998) found that turbid meltwater plume constitutes an ecological stress. Meanwhile, oxygen and carbon dioxide transport from the sea surface to the bottom by brines possibly promoted dissolution of calcareous foraminiferal tests thus contributing to their scarcity in Unit II sediments. Peaks of foraminiferal abundance found in St. Anna and Franz Victoria troughs likely indicate Atlantic water penetration into the Barents Sea (Polyak and Solheim, 1994; Lubinski et al., 1996, 2001; Hald et al., 1999). We interpret occurrence of benthic foraminifers at some Unit II levels in cores ASV 1183 and ASV 1200, as episodes of productivity increase possibly related to longer ice-free seasons in the southern and central BS.

6.2.4. The Holocene marine environments (Unit I)

The onset of the Holocene is marked by a distinct facies change that reflects the transition from glacio-

marine to marine environment in the open BS. The facies change roughly corresponding to the chronostratigraphic Pleistocene–Holocene boundary (10 ^{14}C ka BP), was possibly somewhat diachronous (Ivanova et al., 2002). This change involves both lithological and biological aspects, as shown by the studied proxy records. Sediment color changes from brownish shades to olive gray with black hydrotroilite inclusions indicating bacterial sulfate reduction. Lamination observed in Unit II disappears at the same level suggesting a change in sedimentation mode from flow deposits to particle by particle and pelletal sedimentation with bioturbation and diffuse layering expressed by uneven iron sulfide distribution. Sandy interbeds disappear, except for the lower Holocene interval in Core ASV 1183 (Fig. 11).

TOC concentration and mass accumulation rates increased owing to a higher production of marine organic matter (Romankevich et al., 2000), as well as abundance and diversity of foraminiferal fauna (e.g. Ivanova et al., 2001, 2002; and data in this paper). This suggests higher biological productivity in the Holocene relative to that during the deglaciation. Macrobenthos inhabited the BS depressions and produced an intense bioturbation of the sediments throughout Unit I. Many authors relate the Holocene increase in productivity to intensified surface and subsurface Atlantic water inflow into the BS resulting from climate warming and development of the thermohaline circulation in the North Atlantic (e.g. Lubinski et al., 1996, 2001; Hald et al., 1999; Duplessy et al., 2001, 2005; Ivanova et al., 2002).

Our coring data presented above, as well as seismic records (e.g. Gataullin et al., 1993, 2001; Pavlidis et al., 2005) support the previous suggestions (e.g. Gurevich, 1995) about a major topographic control on the Holocene facies diversity in the BS. First of all, this concerns variations in thickness of the Unit I sediments and their grain-size distribution which, in turn, depend on redistribution of rather uniform fine-grained suspended matter content un the near-bottom nepheloid layer. We did not find any distinct evidence for increased sediment flux related to the marginal ice zone (MIZ) in the thickness variation of Holocene sediments from the open BS. The ice-rafted fine-grained material is likely released and dispersed in the surface water throughout the wide seasonal sea ice zone. However, increased thicknesses of Holocene sediments and enhanced productivity are noted near the MIZ in the south-eastern BS (e.g. Voronina et al., 2001).

As shown above (Figs. 2–4), and confirmed by results of several later expeditions, relatively thick (1–5 m) Holocene sediments occur only in local depressions serving as suspended matter traps. Wide areas in the BS deep basins are covered with thin (commonly less than 1 m) fine-grained Holocene sediments, whereas non-deposition environments with local accumulations of IRD dominate on submarine rise summits.

The Holocene depression facies can be subdivided into three types according to their foraminiferal fauna.

Facies type 1 comprises cores with almost continuous benthic foraminiferal records and with relatively abundant benthic (in some cases also planktic) foraminiferal fauna. It is represented in the eastern branch of the Franz Victoria Trough by our core ASV 880 (Fig. 6, Murdmaa and Ivanova, 1999; Duplessy et al., 2001; Ivanova and Murdmaa, 2001) and by several cores from earlier expeditions (Lubinski et al., 1996, 2001). Cores from the Persey Trough (ASV 858, ASV 1200, ASV 1221) belong to the same facies type, although contain a few planktic foraminifers (Table 5). Both regions are within the seasonal sea-ice zone, near the summer (Franz Victoria Trough) and winter (Persey Trough) ice margins, and are characterized by a presence of subsurface Atlantic water. The permanent occurrence of *C. teretis* in several cores from the northern BS suggests intensified penetration of Atlantic water (Polyak and Solheim, 1994; Lubinski et al., 1996, 2001; Hald et al., 1999; Ivanova and Murdmaa, 2001). The Atlantic water inflow possibly promotes the productivity, and thus provides favorable conditions for the development of foraminiferal fauna (e.g. Ivanova et al., 2001). Near-MIZ productivity blooms may also contribute to the abundance of foraminiferal fauna. High sedimentation rates and intense bioturbation lead to fast burial of foraminiferal tests and contribute to their good preservation.

Facies type 2, widespread in the northern and eastern parts of the study area, includes Holocene sections comprising alternating intervals with rich foraminiferal assemblages and almost barren ones. It occurs in narrow deep troughs to the south of the Franz Josef Land, which are filled with Arctic water (cores ASV 883, ASV 891, ASV 902), and in the Western Novaya Zemlya Trough (cores ASV 1310, ASV 1006, ASV 1157), where the transformed Barents Sea water mass dominates in the water column. Core ASV 1183 likely belongs to this type as well. The low foraminiferal abundance and appearance of barren intervals, especially in the Late Holocene sections from the Western Novaya Zemlya Trough, are evidence of low surface water productivity and/or enhanced dissolution (Ivanova et al., 2002; Levitan et al., 2003b). Intense brines activity assumed in the south-eastern BS (Duplessy et al., 2005; Ivanov and Shapiro, 2005), which favors CO_2 production in

bottom water and sediment pore water (Steinsund and Hald, 1994), likely contributed to the dissolution. High values of *P. orbiculare*, considered as an indicator of freshening (Ivanova, 2002; Polyak et al., 2002), in the Early Holocene of Core ASV 1157 reflect a decrease in bottom-water salinity owing to the enhanced Pechora River runoff (Levitan et al., 2003b).

Facies type 3 comprises thin, almost or totally barren, Holocene sections from deep-water plains and hills (cores ASV 875, ASV 877, ASV 897, ASV 1190, ASV 1302). Slow sedimentation rates and winnowing out of sediments by bottom currents possibly result in strong dissolution of calcareous foraminiferal tests. Restricted food supply owing to low organic matter accumulation rates may also lead to ecological stress for benthic foraminiferal fauna in such an environment.

7. Conclusions

The sedimentary history of the BS is dominated by terrigenous sedimentation under a topographic control. Two major terrigenous material components, the fine-grained and the coarse-grained, demonstrate relatively independent behavior during material delivery, sediment transport and final deposition. Glacier meltwater discharge strongly dominated in the fine-grained material supply during deglaciation and was still significant during the Holocene, along with sea ice rafting, remote river discharge, and other sources. Various gravity flows, bottom currents, and dense bottom water (sea ice freezing brine) cascades redistribute the fine-grained suspended material from submarine rises and deep planes to local shelf depressions. Coarse fractions mainly derived from glacial erosion are distributed by iceberg and sea ice rafting and partially by gravity flows. A minor contribution of biogenic processes to the sedimentation (organic matter accumulation and decay, burial of fossils, pelletal sedimentation, bioturbation, and bacterial activity) became significant only in the Holocene due to a sharp increase in productivity of surface waters.

In shelf depressions, sediment cores show a succession of lithostratigraphic units, which reflect four major development stages of sedimentary environments:

- Unit IV, glacial environment, when moraine (glacial till) formation and glacier erosion predominated;
- Unit III, proximal glaciomarine environment that marks the beginning of the deglaciation, with facies of iceberg turbated sediment, mixed iceberg-rafted/glacier meltwater sediments, and gravity flow deposits;
- Unit II, distal glaciomarine environment dominated by deposition from gravity flows, while iceberg rafting ceased, indicating that the glacier front retreated away from the central areas of the BS; marine productivity was extremely low, but rare benthic foraminifers indicate the sporadic penetration of Atlantic waters into the BS;
- Unit I, marine environment during the Holocene, with a considerable contribution of sea ice rafting, glacier meltwater discharge, and biogenic processes. Facies variability of the Holocene sediments depends mainly on variations of material supply, activity of bottom currents resulting in suspended matter redistribution, and biological productivity controlled by Atlantic water inflow, as well as the sea ice margin.

Acknowledgements

The cores were collected during cruises of *R/V Akademik Sergei Vavilov* financed by P.P. Shirshov Insititute of Oceanology, Russian Academy of Sciences (IO RAS). We acknowledge RFBR-CNRS (PICS grant 98-05-22029), CEA, CNRS-INSU and EU-DGXII (ENVC-CT97-0643) for financial support. At the final stage, this work was supported by the Russian Foundation for Basic Research, project 06-05-64803a. We are grateful to N. Tikhonova and I. Sadovnikova for drawing figures, to V. Kazakova and A. Rudakova for grain size and heavy minerals analyses, to A. Gordeev for TOC analyses, to L. Merklin, A. Byakov, and E. Belousova for supplying the seismic records, to N. Kucheruk for Bivalve determination, to N. Bubenchikova for help in foraminiferal samples preparing (all from IO RAS), as well as to M. Paterne, N. Tisnerat and E. Kaltnecker for performing the AMS ^{14}C analyses with the Gif-sur-Yvette Tandetron.

References

Aibulatov, N.M., Matyushenko, V.A., Shevchenko, V.P., Politova, N.V., 1999. New data on structure of lateral suspended matter fluxes in the periphery of the Barents Sea. Geoecology 6, 526–540.

Alekhin, S.V., 1993. Structure of Mesozoic deposits of the Barents Sea according to seismic data. In: Bezmaternykh, E.F., Senin, B.V., Shipilov, E.V. (Eds.), Osadochnyi chekhol Zapadno-Arkticheskoi metaplatformy. (Sedimentary cover of the West-Arctic metaplatform). Sever, Murmansk, pp. 110–116 (in Russian).

Biscaye, P.E., 1965. Mineralogy and Sedimentation of Recent Deep-Sea Clay in the Atlantic Ocean and Adjacent Seas and Oceans. Geol. Soc. Amer. Bull. 76, 803–832.

Bogdanov, Yu.A., Murdmaa, I.O., Gurvich, E.G., Pimenov, N.V., Pavlova, G.A., Karpenko, A.A., Vlasova, I.E., Plishkin, A.N.,

2001. The study of upper part of Barents Sea sedimentary layer for sedimentation history outline and paleoceanographic reconstructions. In: Lisitsyn, A.P., Vinogradov, M.E., Romankevich, E.A. (Eds.), Opyt sistemnykh okeanologioheskikh issledovanii v Arctike. (Experience of system oceanologic studies in the Arctic). Nauchnyi Mir, Moscow, pp. 598–615 (in Russian, with English abstr.).

Byshev, V.I., Galerkin, L.I., Gorotov, A.S., 2001. Thermohaline structure of the Barents Sea waters in September 1998. In: Lisitsyn, A.P., Vinogradov, M.E., Romankevich, E.A. (Eds.), Opyt sistemnykh okeanologioheskikh issledovanii v Arctike. (Experience of system oceanologic studies in the Arctic). Nauchnyi Mir, Moscow, pp. 102–109 (in Russian, with English abstr.).

Djenynk, S.L., 1990. Non-periodical and summarized currents. Gidrometeorologiya i gidrokhimiya morei SSSR: 1. Barentsevo more. Vyp.1. Gidrometeorologicheskie uslovia. (Hydrometeorology and hydrochemistry of USSR. 1.Barents Sea. Issue 1. Hydrometeorological conditions). Gidrometizdat, Leningrad, pp. 33–40 (in Russian).

Dowdeswell, J.A., Drewry, D.J., 1989. The dynamics of Austfonna, Nordaustlandet, Svalbard: surface velocities, mass-balance, and subglacial meltwater. Ann. Glaciol. 12, 37–45.

Dowdeswell, J.A., Cromack, M., 1991. Behaviour of a glacier-derived suspended sediment plume in a small Arctic inlet. Journal of Geology 99, 111–123.

Dowdeswell, J.A., Whittington, R.J., Marienfeld, P., 1994. The origin of massive diamicton facie by iceberg rafting and scouring, Scoresby Suud, East Greenland. Sedimentology 41, 21–35.

Dowdeswell, J.A., Whittington, R.J., Jenleins, A.E., Andrews, J.T., Mackensen, A., Marienfeld, P., 2000. An origin of laminated glacimarine sediments through sea-ice build-up and suppressed iceberg rafting. Sedimentology 47, 557–576.

Duplessy, J.-C., Ivanova, E.V., Murdmaa, I.O., Paterne, M., Labeyrie, L., 2001. Holocene paleoceanography of the Northern Barents Sea and variations of the northward heat transport by the Atlantic Ocean. Boreas 30 (1), 2–16.

Duplessy, J.-C., Cortijo, E., Ivanova, E., Labeyrie, L., Levitan, L., Murdmaa, I., Paterne, M., 2005. Paleoceanography of the Barents Sea during the Holocene. Paleoceanograph 20, PA 4004. doi:10.1029/2004PA001116.

Elverhoi, A., Solheim, A., 1983. The Barents Sea Ice Sheet—a sedimentological discussion. Polar Res. 1, 23–42.

Elverhoi, A., Pfirman, S.L., Solheim, A., Larsen, B.B., 1989. Glaciomarine sedimentation in epicontinental seas exemplified by the Northern Barents Sea. Mar. Geol. 85, 225–250.

Elverhoi, A., Fjeldskaar, W., Solheim, A., Nyland-Berg, M., Russwurm, L., 1993. The Barents Sea Ice Sheet—A model of its growth and decay during the last ice maximum. Quat. Sci. Rev. 12 (10), 863.

Elverhoi, A., Andersen, E.S., Dokken, T., Hebbeln, D., Spielhagen, R., Svendsen, J.I., Sorflaten, M., Rornes, A., Hald, M., Forsberg, C.F., 1995. The growth and decay of the Late Weichselian Ice Sheet in Western Svalbard and adjacent areas based on provenance studies of marine sediments. Quat. Res. 44, 303–316.

Gataullin, V., Polyak, L., 1997. Morainic Ridge complex, Eastern Barents Sea. In: Davis, T.A., et al. (Eds.), Glaciated Continental Margins: An Atlas of Acoustic Images. Chapman & Hall, London, pp. 82–83.

Gataullin, V., Polyak, L., Epstein, O., Romanyuk, B., 1993. Glacigenic deposits of the Central Deep: a key to the Late Quaternary evolution of the eastern Barents Sea. Boreas 22, 47–58.

Gataullin, V., Mangerud, J., Svendsen, J.I., 2001. The extend of the Late Weichselian ice sheet in the southeastern Barents Sea. Glob. Planet. Change 31, 453–474.

Gilbert, R., 1983. Sedimentary processes of Canadian Arctic fjords. Sediment. Geol. 36, 147–175.

Gurevich, V.I., 1995. Recent sedimentogenesis and environment on the Arctic shelf of the Western Eurasia. Meddelelser, vol. 131. Oslo.

Hald, M., Danielsen, Ò.Ê., Lorentzen, S., 1989. Late Pleistocene and Holocene benthic foraminiferal distribution in the southwestern Barents Sea: paleoenvironmental implications. Boreas 18, 367–388.

Hald, M., Sættem, J., Nesse, E., 1990. Middle and Late Weichslian stratigraphy in shallow drillings from the southwestern Barents Sea: foraminiferal, amino acid and radiocarbon evidence. Nor. Geol. Tidsskr. 70, 241–257.

Hald, M., Dokken, T., Hagen, S., 1996. Paleoceanography of the European Arctic margin during the last deglaciation. In: Andrews, J.T., Austin, W.E.N., Bergsten, H., Jennings, A.E. (Eds.), Late Quaternary Paleoceanography of the North Atlantic Margins. Geol. Soc. Spec. Publ., Boulder, vol. 111, pp. 275–287.

Hald, M., Kolstad, V., Polyak, L., Forman, S.L., Herlihy, F.A., Ivanov, G., Nescheretov, A., 1999. Late glacial and Holocene paleoceanography and sedimentary environments in the Saint Anna Trough, Eurasian Arctic Ocean margin. Palaeogeogr. Palaeoclimatol. Palaeoecol. 146, 229–249.

Ignatenko, E.A., Cheredeev, S.I., 1993. Structural characteristics of the Barents Sea sedimentary cover. In: Bezmaternykh, E.F., Senin, B.V., Shipilov, E.V. (Eds.), Osadochnyi chekhol Zapadno-Arkticheskoi metaplatformy. (Sedimentary cover of the West-Arctic metaplatform). Sever, Murmansk, pp. 26–34 (in Russian).

Ivanova, E.V., 1999. Foraminiferal assemblages of the Barents and Kara seas: response to Holocene environmental changes. In: Yudakhin, F.N. (Ed.), Geodynamics and Geoecology. Inst. of the Ecological Problems of the North, Ural Department of the Russian Academy of Sciences, Arkhangelsk, pp. 140–142.

Ivanova, E.V., 2002. Holocene foraminiferal assemblages of Barents and Kara seas: a response to paleoceanographic changes. EMMM'2002 Program and Abstracts, Vienna, Austria, pp. 106–107.

Ivanova, E.V., Murdmaa, I.O., 2001. Postglacial paleoceanography of the Northern Barents Sea. In: Lisitsyn, A.P., Vinogradov, M.E., Romankevich, E.A. (Eds.), Opyt sistemnykh okeanologioheskikh issledovanii v Arctike. (Experience of system oceanologic studies in the Arctic). Nauchnyi Mir, Moscow, pp. 542–552 (in Russian, with English abstr.).

Ivanov, V.V., Shapiro, G.I., 2005. Formation of a dense water cascade in the marginal ice zone in the Barents Sea. Deep-Sea Res. I 52, 1699–1717.

Ivanova, E.V., Duplessy, J.C., Paterne, M., Murdmaa, I.O., Levitan, M.A., Vetrov, A.A., Romankevich, E.A., Khusid, T.A., 2001. The influence of climate and thermohaline circulatiopn on the productivity of the Eastern Barents Sea during the Holocene. ICP VII Program and Abstracts, Sapporo, Japan, p. 125.

Ivanova, E.V., Murdmaa, I.O., Duplessy, J.-C., Paterne, M., 2002. Late Weichselian to Holocene Paleoenvironments of the Barents Sea. Glob. Planet. Change 34 (3–4), 209–218.

Jones, G.A., Keigwin, L.D., 1988. Evidence from Fram Strait (78°N) for early deglaciation. Nature 336, 56–59.

Kalinenko, V.V., 1985. Sedimentational features in the Central Barents Sea. Geologiya i geomorfologiya shelfov i materikovyh sklonov. (Geology and geomorphology of shelves and continental slopes). Nauka, Moscow, pp. 101–112 (in Russian).

Kalinenko, V.V., 2001. Clay minerals in sediments of Arctic seas. Lithol. Miner. Resour. 4, 418–429 (English translation).

Korsun, S., Hald, M., 1998. Modern benthic foraminifera off Novaya Zemlya tidewater glaciers, Russian Arctic. Arct. Alp. Res. 30, 61–77.

Lambeck, K., 1995. Constrains on the late Weichselian ice sheet over the Barents Sea from observations of raised shorelines. Quat. Sci. Rev. 14, 1–16.

Lambeck, K., Yokoyama, Y., Jonston, P., Purcell, A., 2000. Global ice volumes at the Last Glacial Maximum and early Late Glacial. Earth Planet. Sci. Lett. 181, 513–527.

Lehman, S.J., 1991. Initiation of Fennoscandian ice-sheet retreat during the last deglaciation. Nature 349, 513–516.

Levitan, M.A., Tarasov, G.A., Bourtman, M.V., Kukina, N.A., 1999. Mineral composition of surface sediments from the St. Anna Trough. Oceanology 39 (6), 903–911 (English translation).

Levitan, M.A., Bourtman, M.V., Dara, O.M., 2003a. Upper Quaternary bottom sediments. In: Romankevich, E.A., Lisitsyn, A.P., Vinogradov, M.E. (Eds.), Pechorskoe more: sistemnye issledovaniya. (The Pechora Sea: Integrated Research). More, Moscow, pp. 263–284. Chapter 11, in Russian, with English abstract.

Levitan, M.A., Belyaev, N.A., Bourtman, M.V., Duplessy, J.-C., Khusid, T.A., 2003b. Holocene sedimentation history in the Southern Novaya Zemlya Trench. Lithol. Miner. Resour. 6, 660–672 (English translation).

Lubinski, D., Korsun, S., Polyak, L., Forman, S.L., Lehman, S.J., Herlihy, F.A., Miller, G.H., 1996. The last deglaciation of the Franz Victoria Trough, northern Barents Sea. Boreas 25, 89–100.

Lubinski, D.J., Polyak, L., Forman, S.L., 2001. Freshwater and Atlantic water inflows to the deep northern Barents and Kara seas since ca 13 ^{14}C ka: foraminifera and stable isotopes. Quat. Sci. Rev. 20, 1851–1879.

Medvedev, V.S., Potekhina, E.M., 1990. Transportation of terrigenous suspension by modern glaciers of Novaya Zemlya to the Barents Sea. In: Aibulatov, N.M. (Ed.), Sovremennye protsessy osadkonakopleniya na shel'fah Mirovogo okeana. (Modern sedimentation processes on shelves of the World Ocean). Nauka, Moscow, pp. 103–110.

Midttun, L., 1985. Formation of dense bottom water in the Barents Sea. Deep-Sea Res. 32, 1233–1241.

Murdmaa, I.O., Ivanova, E.V., 1999. Postglacial sedimentation history in shelf depressions of the Barents sea. Lithol. Miner. Resour. 6, 576–595 (English translation).

Murdmaa, I.O., Ivanova, E.V., Pimenov, N.V., 1998. Paleoceanographic changes in the Barents Sea: interrelations with global thermohaline circulation. In: Proc. 6 Int. Conf. on Paleoceanography. Lisbon, Portugal, p. 71.

Murdmaa, I.O., Polyak, L., Ivanova, E.V., Khromova, N.V., 2004. Paleoenvironments in the Russkaya Gavan' Fjord (NW Novaya Zemlya) during the Last Millenium. Palaeogeogr. Palaeoclimatol. Palaeoecol. 209, 141–154.

Nürnberg, D., Levitan, M., Pavlidis, Yu., Shelekhova, E., 1995. Distribution of clay minerals in surface sediments from the eastern Barents and south-western Kara seas. Geol. Rundsch. 84, 665–682.

Ó'Cofaigh, C., Dowdeswell, J.A., 2001. Laminated sediments in glacimarine environments: diagnostic criteria for their interpretation. Quat. Sci. Rev. 20, 1411–1436.

Pavlidis, Yu.A., Polyakova, E.I., 1997. Late Pleistocene and Holocene depositional environments and paleoceanography of the Barents Sea: evidence from seismic and biostratigraphic data. Mar. Geol. 143, 189–205.

Pavlidis, Yu.A., Murdmaa, I.O., Ivanova, E.V., Artemyev, A.V., Belousov, M.A., 2001. Whether the Novaya Zemlya and Franz Jozef Land ice sheets were connected 18 kyr ago? In: Lisitsyn, A.P., Vinogradov, M.E., Romankevich, E.A. (Eds.), Opyt sistemnykh okeanologioheskikh issledovanii v Arctike. (Experience of system oceanologic studies in the Arctic). Nauchnyi Mir, Moscow, pp. 618–632 (in Russian, with English abstr.).

Pavlidis, Yu.A., Bogdanov, Yu.A., Levchenko, O.V., Murdmaa, I.O., Tarasov, G.A., 2005. New data on the paleoenvironments in the Barents Sea at the end of Valdai Glaciation. Oceanology 45 (1), 92–106 (English translation).

Petelin, V.P., 1967. Granulometricheskii analiz morskih donnyh osadkov (Granulometrical analysis of marine sediments). Nauka, Moscow (in Russian).

Polyak, L., Mikhailov, V., 1996. Post-glacial environments of the southeastern Barents Sea: foraminiferal evidence. In: Andrews, J. T., et al. (Eds.), Late Quaternary Paleoceanography of the North Atlantic Margins. Geol. Soc. Spec. Publ., vol. 111, pp. 323–337.

Polyak, L., Solheim, A., 1994. Late-and postglacial environments in the northern Barents Sea west of Franz Josef Land. Polar Res. 13 (2), 197–207.

Polyak, L., Lehman, S.J., Gataullin, V., Jull, A.C.T., 1995. Two-step deglaciation of the southeastern Barents Sea. Geology 23, 567–571.

Polyak, L., Forman, S.L., Herlihy, F.A., Ivanov, G., Krinitsky, P., 1997. Late Weichselian deglacial history of the Svyataya (Saint) Anna Trough, northern Kara Sea, Arctic Russia. Mar. Geol. 143, 169–188.

Polyak, L., Gataullin, V., Okuneva, O., Stelle, V., 2000. New constrains on the limits of the Barents-Kara ice sheet during the Last Glacial Maximum based on borehole stratigraphy from the Pechora Sea. Geology 28, 611–614.

Polyak, L., Korsun, S., Febo, L., Stanovoy, V., Khusid, T., Hald, M., Paulsen, B.E., Lubinski, D.A., 2002. Benthic foraminiferal assemblages from the Southern Kara Sea, a river-influenced arctic marine environment. J. Foraminiferal Res. 32, 252–273.

Romankevich, E.A., Vetrov, A.A., Vinogradov, M.E., Vedernikov, V.I., 2000. Some Elements of the Carbon Cycle in the Russian Arctic Seas. Fluxes of Carbon from Land, Carbon in Bottom Sediments, Elements of Budget. Oceanology 40 (3), 363–372.

Sættem, J., Poole, D.A.R., Ellingsen, K.L., Sejrup, H.P., 1992. Glacial geology of outer Bjørnøjrenne, Southwestern Barents Sea. Mar. Geol. 103, 15–51.

Sarnthein, M., Jansen, E., Weinelt, M., Arnold, M., Duplessy, J., Erlenkeuser, C., Flatoy, H., Johannessen, A., Johannessen, G., Jung, T., Koc, S., Labeyrie, N., Maslin, L., Pflaumann, M., Schulz, U., 1995. Variations in Atlantic surface ocean paleoceanography, 50–80°N: a time-slice record of the last 30,000 years. Paleoceanography 10, 1063–1094.

Sarnthein, M., Stattegger, K., Dreger, D., Erlenkeuser, H., et al., 2000. Fundamental Modes of Abrupt Changes in North Atlantic Circulation and Climate over the last 60 ky – Concepts, Reconstruction and Numerical Modeling. In: Schäfer, P., Ritzrau, W., Schlüter, M., Thiede, J. (Eds.), The Northern North Atlantic: A Changing Environment. Springer, Berlin, pp. 265–410.

Shelekhova, E.S., 1998. Regularities of clay minerals distribution in the surface layer of sediments from the Barents and Kara seas. PhD thesis (unpublished), Shirshov Institute of Oceanology, RAS (in Russian).

Shevchenko, V.P., 2003. The influence of aerosols on the oceanic sedimentation and environmental conditions in the Arctic.

Berichte zur Polar-und Meeresforschung, vol. 464. AWI, Bremerhaven, p. 149.
Sigmond, E.M.O. 1992. "Bedrock map of Norway and adjacent ocean areas", Scale 1: 3 million. Geological Survey of Norway.
Solheim, A., Musatov, E., Heinz, N., 1998. Geological aspects of Franz Josef Land and the northernmost Barents Sea. The Northern Barents Sea Geotraverse. Meddelelser, vol. 131. Oslo.
Spielhagen, R.F., Erlenkeuser, H., Siegert, C., 2005. History of freshwater runoff across the Laptev Sea (Arctic) during the last deglaciation. Glob. Planet. Change 48, 187–207.
Stein, R., Grobe, H., Wahsner, M., 1994. Organic carbon, carbonate and clay mineral distributions in eastern central Arctic Ocean surface sediments. Mar. Geol. 119, 269–285.
Stein, R., Dittmers, K., Fahl, K., Kraus, M., Matthiessen, J., Niessen, F., Pirrung, M., Polyakova, Ye., Schoster, F., Steinke, T., FƏtterer, D.K., 2004. Arctic (Palaeo) River Discharge and Environmental Change: evidence from Holocene Kara Sea Sedimentary Records. Quat. Sci. Rev. 23, 1485–1511.
Steinsund, P.I., Hald, M., 1994. Recent calcium carbonate dissolution in the Barents Sea, Paleaoceanographic applications. Mar. Geol. 117, 303–316.
Stuiver, M., Reimer, P.J., 1993. Extended ^{14}C data base and revised CALIB 3.0 ^{14}C age calibration program. Radiocarbon 35, 215–230.
Svendsen, J.I., Astakhov, V.I., Bolshiyanov, D.Y., Demidov, I., Dowdeswell, J.A., Gataullin, V., Hjort, Ch., Hubberten, H.W., Larsen, E., Mangerud, J., Melles, M., Möller, P., Saarnisto, M., Siegert, M.J., 1999. Maximum extent of the Eurasian ice sheets in the Barents and Kara Sea region during the Weichselian. Boreas 28, 234–242.
Svendsen, J.I., Alexanderson, H., Astakhov, V.I., Demidov, I., Doudeswell, J.A., Funder, S., Gataullin, V., Hendriksen, M., Hjort, C., Henmark-Nielsen, M., Hubberten, H.W., Ingolffson, O., Jakobsson, M., Kjar, K.H., Larsen, E., Lokrantz, H., Luukka, J.P., Lysa, A., Mangerud, J., Matiouchkov, A., Murray, A., Moller, P., Niessen, F., Nikolskaya, O., Polyak, L., Saarnisto, M., Siegert, C., Siegert, M.J., Spielhagen, R.F., Stein, R., 2004a. Late Quaternary ice sheet history of northern Eurasia. Quat. Sci. Rev. 23 (11–12), 1229–1271.
Svendsen, J.I., Gataullin, V., Mangerud, J., Poljak, L., 2004b. The glacial history of the Barents and Kara Sea region. In: Ehlers, J., Gibbard, P. (Eds.), Quaternary Glaciations— Extent and Chronology, vol. 1. Elsevier, Amsterdam, pp. 369–378.
Thiede, J., Mangerud, J., 1999. New Map Revises Extent of Last Ice Sheet Over Barents and Kara Seas. EOS Trans. 80 (42), 493–494.
Vinje, T., 1985. Drift, composition, morphology and distribution of the sea ice fields in the Barents Sea. Nor. Polarinst. Skr. 179C, 1–26.
Viscosi-Shirley, C., Mammone, K., Pisias, N., Dymond, J., 2003. Clay mineralogy and multi-element chemistry of surface sediments on the Siberian-Arctic shelf: implications for sediment provenance and grain size sorting. Cont. Shelf Res. 23, 1175–1200.
Voronina, E., Polyak, L., De Vernal, A., Peyron, O., 2001. Holocene variations of sea-surface conditions in the southeastern Barents Sea, reconstructed from dinoflagellate cyst assemblages. J. Quat. Sci. 16 (7), 717–726.
Vorren, T.O., 1992. Glaciation of the Barents Sea—an overviw. Sver. Geol. Unders. Ser. Ca Avh. Upps. 81, 367–372.
Vorren, T.O., Laberg, J.S., 1996. Late glacial air temperature, oceanographic and ice sheet interactions in the southern Barents Sea region. In: Andrews, J.T., Austin, W.E., Bergsten, W.E.N., Jennings, A.E. (Eds.), Late Quaternary Paleoceanography of the North Atlantic Margins. Geol. Soc. Spec. Publ., vol. 111, pp. 303–321.
Vorren, T.O., Hald, M., Edvardsen, M., Lind-Hansen, O.W., 1983. Glacigenic sediments and sedimentary environments on continental shelves: general principles with a case study from Norwegian shelf. In: Ehlers, J. (Ed.), Glacial Deposits in Northern Europe. A.A. Balkema, Roterdam, pp. 61–73.
Vorren, T.O., Hald, M., Thomson, E., 1984. Quaternary sediments and environments on the continental shelf off northern Norway. Mar. Geol. 57, 229–257.
Vorren, T.O., Lebesbye, E., Angreassen, K., Larsen, K.-B., 1989. Glacigenic sediments on a passive continental margin as examplified by the Barents Sea. Mar. Geol. 85, 251–272.
Wahsner, M., Muller, K., Stein, R., Ivanov, G., Levitan, M., Shelekhova, E., Tarasov, G., 1999. Clay-mineral distribution in surface sediments of the Eurasian Arctic Ocean and continental margin as indicator for source areas and transport pathways — a synthesis. Boreas 28, 215–233.
Weinelt, M.S., Sarnthein, M., Vogelsang, E., Erlenkeuser, H., 1991. Early decay of the Barents Shelf Ice Sheet-spread of stable isotope signals across the eatern Norwegian Sea. Nor. Geol. Tidsskr. 71, 137–140.
Wright, P.L., 1974. Recent sediments from thesouthwestern Barents Sea. Mar. Geol. 16, 51–81.
Zubakin, G.K., 1990. Sea-ice conditions and location of the ice margin. Gidrometeorologiya i gidrokhimiya morei SSSR. 1. Barentsevo more. Vyp.1 Gidrometeorologicheskie usloviya, Hydrometeorology and hydrochemistry of USSR: 1.Barents Sea. Issne 1. Hydrometeorological conditions. Gidrometizdat, Leningrad, pp. 250–254 (in Russian).